Cell Transplantation, Vol. 23, pp. 1305–1319, 2014
Printed in the USA.

0963-6897/14 $90.00 + .00
DOI: http://dx.doi.org/10.3727/096368913X665602
E-ISSN 1555-3892
www.cognizantcommunication.com

Improvement of Cardiac Stem Cell Sheet Therapy for Chronic Ischemic Injury by Adding Endothelial Progenitor Cell Transplantation: Analysis of Layer-Specific Regional Cardiac Function

Sokichi Kamata,* Shigeru Miyagawa,* Satsuki Fukushima,* Satoshi Nakatani,† Atsuhiko Kawamoto,‡ Atsuhiro Saito,* Akima Harada,* Tatsuya Shimizu,§ Takashi Daimon,¶ Teruo Okano,§ Takayuki Asahara,‡ and Yoshiki Sawa*

*Department of Cardiovascular Surgery, Osaka University Graduate School of Medicine, Suita, Japan
†Division of Functional Diagnostics, Department of Cardiovascular Medicine, Osaka University Graduate School of Medicine, Suita, Japan
‡Division of Vascular Regeneration Therapy, Institute of Biomedical Research and Innovation, Kobe, Japan
§Institute of Advanced Biomedical Engineering and Science, Tokyo Women's Medical University, Tokyo, Japan
¶Department of Biostatistics, Hyogo College of Medicine, Nishinomiya, Hyogo, Japan

The transplantation of cardiac stem cell sheets (CSC sheets) is a promising therapeutic strategy for ischemic cardiomyopathy, although potential ischemia in the transplanted area remains a problem. Injected endothelial progenitor cells (EPCs) can reportedly induce angiogenesis in the injected area. We hypothesized that concomitant CSC sheet transplantation and EPC injection might show better therapeutic effects for chronic ischemic injury model than the transplantation of CSC sheets alone. Scaffold-free CSC sheets were generated from human c-kit-positive heart-derived cells. A porcine chronic ischemic injury model was generated by placing an ameroid constrictor around the left coronary artery for 4 weeks. The animals then underwent a sham operation, epicardial transplantation of CSC sheet over the ischemic area, intramyocardial injection of EPCs into the ischemic and peri-ischemic area, or CSC sheet transplantation plus EPC injection. The efficacy of each treatment was then assessed for 2 months. Speckle-tracking echocardiography was used to dissect the layer-specific regional systolic function by measuring the radial strain (RS). The epicardial RS in the ischemic area was similarly greater after treatment with the CSC-derived cell sheets alone (19±5%) or in combination with EPC injection (20±5%) compared with the EPC only (9±4%) or sham (7±1%) treatment. The endocardial RS in the ischemic area was greatest after the combined treatment (14±1%), followed by EPC only (12±1%), compared to the CSC only (11±1%) and sham (9±1%) treatments. Consistently, either epicardial CSC sheet implantation or intramyocardial EPC injection yielded increased capillary number and reduced cardiac fibrosis in the ischemic epicardium or endocardium, respectively. Concomitant EPC injection induced the migration of transplanted CSCs into the host myocardium, leading to further neovascularization and reduced fibrosis in the ischemic endocardium, compared to the CSC sole therapy. Transplantation of CSC sheets induced significant functional recovery of the ischemic epicardium, and concomitant EPC transplantation elicited transmural improvement in chronic ischemic injury.

Key words: Cardiac stem cells (CSCs); Endothelial progenitor cells (EPCs); Chronic ischemic injury; Strain imaging; Left ventricular remodeling

INTRODUCTION

Transplantation of somatic tissue-derived stem cells has been shown to be a feasible, safe, and potentially effective treatment for advanced cardiac failure in clinical settings (6,32). In particular, cardiac stem cells (CSCs), represented by c-kit-positive cells in the myocardium, can play a central role in healing the damaged myocardium, through their direct differentiation in situ, the recruitment of circulating stem/progenitor cells, or the paracrine release of cardioprotective factors (9,12,30). CSC transplantation is therefore considered a promising treatment for advanced cardiac failure, although the optimal method for cell delivery into the heart is still under debate (7).

The transplantation of scaffold-free cell sheets was shown to enhance the retention and survival of the transplanted cells and to minimize the risks of cell delivery-related myocardial damage that leads to arrhythmogenicity, thus showing good therapeutic potential (5,20,33). However,

Received July 26, 2012; final acceptance March 17, 2013. Online prepub date: April 3, 2013.
Address correspondence to Professor Yoshiki Sawa, Department of Cardiovascular Surgery, Osaka University Graduate School of Medicine, 2-2 Yamadaoka, Suita, Osaka 565-0871, Japan. Tel: +81-6-6879-3154; Fax: +81-6-6879-3163; E-mail: sawa-p@surg1.med.osaka-u.ac.jp

concerns remain regarding the integration of the transplanted cells into the myocardium, which would have a direct impact on regional cardiac function, and the potential for ischemia in the transplanted cell sheet, which would limit its therapeutic potential. On the other hand, endothelial progenitor cells (EPCs) have been shown to induce neoangiogenesis in the ischemic/infarcted myocardium and to activate residential CSCs to enhance healing and/or regeneration of the damaged myocardium (11,13,31). The intramyocardial injection of EPCs is thus another promising treatment for enhancing myocardial regeneration and possibly supporting the cellular function of transplanted CSCs (16).

We thus hypothesized that CSC transplantation by the cell sheet technique might induce cardiomyogenic differentiation in situ, reverse left ventricular (LV) remodeling, and improve functional recovery in ischemic injury model and that these therapeutic effects might be enhanced by the concomitant transplantation of EPCs, which could have different effects on the damaged myocardium from CSCs.

Several lines of evidence suggested that region-specific, especially layer-specific, LV function assessed by recently developing modalities may be superior to globally measured ejection fraction (EF) in predicting myocardial recovery after a wide range of medical and surgical treatment (3,14). Here we used a porcine chronic ischemic injury model to dissect the layer-specific functional effects of these two types of cell transplantation.

MATERIALS AND METHODS

All human and animal studies were carried out with the approval of the institutional ethical committee. Human samples were collected under written informed consent. The investigation conforms to the Principles of Laboratory Animal Care formulated by the National Society for Medical Research and the NIH guidelines for the care and use of laboratory animals. All experimental procedures and evaluations were carried out in a blinded manner.

Isolation and Cultivation of C-Kit-Positive Cells From Human Cardiac Tissue

Human normal right atrial tissues were obtained from a 53-year-old female patient with dilated cardiomyopathy at Osaka University Hospital. The isolation method was as published recently (6). Briefly, after dissecting fat and fibrous tissue, the sample was cut into small pieces (<1 mm^3) and suspended in 8 ml Ham's F12 medium (Wako Pure Chemical Inc., Osaka, Japan) containing 0.2% collagenase (17454; Serva Electrophoresis, Heidelberg, Germany). After digestion, cells were plated in culture dishes (353003; BD Falcon, Franklin Lakes, NJ, USA) containing Ham's F12 supplemented with 10% fetal bovine serum (FBS; SH30406.02; Hyclone, Thermo Scientific, Waltham, MA, USA), 10 ng/ml recombinant human basic fibrobrast growth factor (bFGF; 100-18B; PeproTech, Rocky Hill, NJ, USA), 0.2 mM L-glutathione (G6013; Sigma-Aldrich, St. Louis, MO, USA), and 5 mU/ml erythropoietin (E5627-10UN; Sigma Aldrich). Subsequently, cells were expanded and subjected to fluorescence-activated cell sorting (FACSAria; BD Biosciences, San Jose, CA, USA) with antibody {cluster of differentiation 117-phycoerythrin [CD117(AC126)-PE]; also known as c-kit or stem cell growth factor receptor, 130-091-735; Miltenyi Biotec, Bergisch Gladbach, Germany} to obtain c-kit-positive CSCs. The sorted c-kit-positive CSCs were cultured until the fifth passage in the above medium (30).

Preparation of CSC Sheet and Endothelial Progenitor Cells

Cultured CSCs were characterized by fluorescence-activated cell sorting (FACS) analysis, labeled by 2 μM DiI-red (Molecular Probes, Eugene, OR, USA) (33), and then incubated on 10-cm thermoresponsive dishes (Cell Seed Inc., Tokyo, Japan) at 37°C for 12 h. The DiI-red-labeled CSCs spontaneously detached from the dish surface following incubation at 20°C for 30 min, yielding a CSC sheet. Each CSC sheet was approximately 42 mm in diameter and 100 μm thick. Granulocyte colony-stimulating factor-mobilized EPCs of human origin (AllCells, MPB-017F; Emeryville, CA, USA) were labeled with 2 μM DiI-blue in vitro (Molecular Probes) (33). The following monoclonal antibodies were used: c-kit allophycocyanin (APC) [A3C6E2 (clone), 130-091-733; MiltenyiBiotec], CD105 PE (FAB10971P; R&D Systems, Minneapolis, MN, USA), CD34 fluorescein isothiocyanate (FITC) (555821, BD Biosciences), CD31 PE (FAB3567P, R&D Systems), 7-aminoactinomycin D peridinin–chlorophyll protein–cyanine 5.5 [7AAD PerCP-Cy5-5; 51-68981E (559925); BD Biosciences], immunoglobulin G1(IgG1)–FITC isotype controls (555748; BD Biosciences), IgG1–APC isotype controls (130-092-214; Miltenyi Biotec), and IgG1–PE isotype controls (IC002P; R&D Systems).

Generation of the Swine Chronic Ischemic Injury Model and Cell Transplantation

A 2.5-mm ameroid constrictor (Tokyo Instruments, Inc., Tokyo, Japan) was placed around the proximal left anterior descending artery via a left thoracotomy in female swine (Clawn miniature, 1 year old, 25 kg; Japan Farm, Inc., Kagoshima, Japan). A total of 65 swines were then cared for in a temperature-controlled individual cage with a daily intake of 5 mg/kg cyclosporin A (Novartis, East Hanover, NJ, USA) (15). Multidetector CT identified 52 pigs that developed a left ventricular ejection fraction (LVEF) between 30% and 40% at 21 days post-ameroid placement. Since eight of these pigs died prior to cell transplantation, a total of 44 pigs were randomly divided

into four treatment groups ($n=11$ in each): sham operation (sham group), CSC sheet transplantation only (CSC-only group), intramyocardial injection of EPCs (EPC-only group), and CSC sheet transplantation plus EPC injection (CSC–EPC group). After a median sternotomy under general anesthesia, three-layered CSC sheet (total 1×10^8 cells) was placed on the epicardium of the ischemic area [left anterior descending (LAD) region] and stitched in place around the edge. EPCs (total 2.5×10^6 cells) were intramyocardially injected into 12 different sites of the ischemic and peri-ischemic area. After the transplantation and/or intramyocardial injection was completed, the pericardium was closed. The pigs were taken care of for 1 day ($n=1$ each), 3 weeks ($n=4$ each), or 8 weeks ($n=6$ each), when they were sacrificed in a humane manner.

Continuous Electrocardiogram Monitoring

The electrocardiogram (ECG) was monitored during 5 days posttreatment with the Holter system (Unique Medical Co., Tokyo, Japan) for swines sacrificed at 8 weeks after cell transplantation ($n=6$ each group). The heart rate and arrhythmia events during the first 24 h were analyzed using software (Softron Co., Tokyo, Japan).

Multidetector CT and Conductance Catheterization

Global LV function was assessed by multidetector computed tomography (CT) at pretreatment and 8 weeks posttreatment ($n=6$ each) and by cardiac catheterization at 8 weeks posttreatment ($n=5$ each). After infusing 45 ml of nonionic contrast agent (Iomeron 350; Eisai Co., Tokyo, Japan) via the ear vein, 5-mm slice images of the entire heart were obtained in the craniocaudal direction using a 16-slice CT scanner (Emotion 16; Siemens, Tokyo, Japan). Every 10% of the R-R interval was reconstructed to calculate the LVEF and end-diastolic/systolic volume (EDV and ESV, respectively) using software (Lexus, Aze Inc., Tokyo, Japan).

Pressure–volume (P-V) cardiac catheterization was performed after median sternotomy by inserting a conductance catheter (Unique Medical) and a microtip catheter transducer (SPR-671; Millar Instruments, Inc., Houston, TX, USA) into the LV cavity. The P-V loop data under stable hemodynamics or inferior vena cava occlusion were analyzed with Integral 3 software (Unique Medical).

Speckle-Tracking Echocardiography and Myocardial Contrast Echocardiography

Short-axis echocardiographic images, obtained using the Artida 4D Echocardiography System (Toshiba Medical Systems Co., Tochigi, Japan) and PST-30SBT transducer, were analyzed by the speckle-tracking method using wall motion-tracking software (Toshiba Medical Systems) (2,4). End-systolic radial strain (RS) values at the mid and apical levels were averaged in a layer-specific manner to measure the endocardial and epicardial wall motion index (WMI), respectively.

Myocardial contrast echocardiography was performed using real-time contrast pulse sequencing operating on the Aplio ultrasound system (Toshiba Medical Systems) (8). Briefly, after an intravenous injection of 20 ml of ultrasound contrast agent (Sonazoid, Daiichi Sankyo Inc., Parsippany, NJ, USA), images in the apical two-chamber view were acquired to score the myocardial opacification using Volmac software (YD Ltd., Nara, Japan).

Histology

Cultured CSCs on eight-well Lab-Tec chamber slides were fixed with 4% paraformaldehyde (163-20145, Wako Pure Chemical Inc.), labeled, and examined by confocal microscopy (FV300, Olympus, Tokyo, Japan). Alexa Fluor-488 phalloidin (Molecular Probes) was used to enhance the background actin filaments. Paraffin-embedded transverse sections at the papillary muscle level were stained with Masson's trichrome (MT; Masson's Trichrome staining kit, Muto Pure Chemicals, Tokyo, Japan), and the amount of interstitial collagen at the entire LV wall was semi-quantified by MetaMorph software (Molecular Devices, Sunnyvale, CA, USA) ($n=6$, in each). In addition, the thickness of the ventricular wall was measured at two points from the LV posterior area and two points from the interventricular septum, and results were expressed as the average of the four points. Five-micrometer cryosections were subjected to either periodic acid-Schiff (PAS) staining (PAS staining kit, Muto Pure Chemicals) or immunohistolabeling. The following primary antibodies were used: rabbit anti-c-kit (1:50; Dako Co., Glostrup, Denmark), rabbit anti-von Willebrand factor (vWF; 1:500; Dako), mouse anti-Ki-67 (1:50; Dako), rabbit anti-connexin 43 (1:200; Sigma Aldrich), mouse anti-cardiac troponin I (cTn-I; 1:100; Abcam Co., Cambridge, UK), mouse anti-stromal cell-derived factor 1(SDF-1; 1:50; Abcam), rabbit anti-vascular endothelial growth factor (VEGF; 1:100; Thermo Scientific), and rabbit anti-insulin-like growth factor 1 (IGF-1; 1:100; Abcam). Capillary density was expressed as the average number of vWF-positive circular structures in five randomly selected sections, corrected for the total area of the tissue section measured. PAS-stained sections were used to determine the cell diameter of the cardiomyocytes at the remote zone. DiI-red-positive cells were traced by MetaMorph software to quantify the area of engrafted clusters of CSC sheet.

Reverse Transcription Polymerase Chain Reaction (RT-PCR)

Total RNA was extracted from the CSCs and the swine heart tissues posttreatment using an RNeasy Kit (Qiagen, Hilden, Germany), then reverse-transcribed using Omniscript Reverse Transcriptase (Qiagen) and

amplified using the Gene Amp® PCR System 9700 (Life Technologies, Tokyo, Japan). The primer pairs were as follows: human-specific kinase insert domain receptor (KDR or VEGF receptor 2) primer sequence, sense CCT CTA CTC CAG TAA ACC TGA TTG GG, antisense TGT TCC CAG CAT TTC ACA CTA TGG; human-specific chemokine C-X-C motif receptor 4 [CXCR4 or stromal-derived factor 1 (SDF-1) receptor] primer sequence, sense ACG TCA GTG AGG CAG ATG, antisense GAT GAC TGT GGT CTT GAG; human glyceraldehyde-3-phosphate dehydrogenase (GAPDH) primer sequence, sense AAT GGG CAG CCG TTA GGA AA, antisense GCG CCC AAT ACG ACC AAA TC; swine-specific SDF-1 primer sequence, sense CCGAACTGTGCCCTTCAGAT, antisense ATAA ACATCCCGCCGTCCTC; swine-specific CXCR-4 primer sequence, sense GCGCAAAGCTCTCAAAACCA, antisense CAGTGGAAAAAGGCAAGGGC; swine-specific VEGF primer sequence, sense GAC GTC TAC CAG CGC AGC TAC T, antisense TTT GAT CCG CAT AAT CTG CAT G; swine-specific IGF-1 primer sequence, sense ACA TCC TCT TCG CAT CTC TTC TAC TT, antisense CCA GCT CAG CCC CAC AGA; swine GAPDH primer sequence, sense CTG CAC CAC CAA CTG CTT AGC, antisense GCC ATG CCA GTG AGC TTC C. The transcript level of GAPDH was used as an endogenous reference. The products from the cultured CSCs were stained with ethidium bromide (Bio-Rad Laboratories, Hercules, CA, USA), separated by electrophoresis (Mupid submarine electrophoresis system, Advance Co. Ltd., Tokyo, Japan) on an agarose gel (Agarose S, Nippon Gene Co., Ltd., Tokyo, Japan), and quantified.

Fluorescence In Situ Hybridization (FISH)

Paraffin-embedded sections were predenatured, dehydrated, and then labeled with deoxyribonucleic acid probes, a Cy3-conjugated probe for human-specific genome, Cy5-conjugated probe for swine-specific genome (Chromosome Science Laboratory, Hokkaido, Japan), and mouse anti-cTn-I or rabbit anti-vWF. The sections were visualized with secondary antibodies conjugated to Alexa fluorochromes. Nuclei were labeled with 4,6-diamino-2-phenylindole (DAPI; Molecular Probes).

Statistical Analysis

Continuous data are summarized as medians with ranges (minimums to maximums) or means ± SEM (standard error of mean) and are plotted in figures with raw values or barplots of the means with symmetric SEM bars, as appropriate. Distributions of the continuous data were checked for normality with the Shapiro–Wilk test and for equality of between-group variances with the Levene test. Normally distributed data were compared between four groups using the analysis of variance (ANOVA), followed by the Tukey multiple comparison for equal variances, or Welch's ANOVA, followed by the Games–Howell multiple comparison for unequal variances. Nonnormally distributed data were compared using the Kruskal–Wallis test, followed by the Steel–Dwass multiple comparison. Normally and nonnormally distributed data before and after treatment were compared using the paired t test and the Wilcoxon signed rank-sum test, respectively. All p values are two-sided, and values of $p<0.05$ were considered to indicate statistical significance. All analyses were performed with the SPSS 11.0J for Windows (SPSS, Chicago, IL, USA) and the R program (http://www.r-project.org/) (10).

RESULTS

Human Atrium-Derived C-Kit-Positive Cells Showed CSC Characteristics In Vitro

The isolated right atrium-derived cells were characterized in vitro by FACS, immunohistolabeling, and RT-PCR analyses. The proportion of c-kit-positive cells at the second passage was 99±4% (Fig. 1A and B). However, as the cells expanded, they lost the primitive phenotype, and more than half of them had the potential to differentiate to the endothelial rather than the cardiomyocyte or smooth muscle cell lineage. The proportion of c-kit-positive cells at the fifth passage was 20±10%, while 34%, 71%, and 99% of them expressed CD34, CD31, and CD105, respectively (Fig. 1C). Immunohistochemistry revealed that approximately 5% of the cells expressed cTn-I in the cytoplasm (Fig. 1D). In addition, RT-PCR clearly revealed the expression of CXCR4 and KDR in the cells (Fig. 1E).

After incubating the cells on temperature-responsive dishes at 37°C for 12 h, CSC sheets were generated by lowering the temperature. Each cell sheet was approximately 42 mm in diameter, and the gap junction protein connexin 43 was expressed between the cells (Fig. 1F). Most of the cells expressed the proliferation marker Ki-67 in their nucleus (Fig. 1G).

Successful Cell Transplantation With Minimal Arrhythmogenicity

A total of 44 pigs underwent treatment, which was performed without any procedure-related mortalities ($n=11$ each). Fatal arrhythmias, such as ventricular tachycardia and fibrillation, or composite ventricular arrhythmias (grades 3–5 in Lown's classification) were not detected in any group during the first 24 h posttreatment, as assessed by Holter ECG monitoring ($n=6$ each) (Table 1). There were no significant differences in the heart rate or number of unifocal premature ventricular/atrial contractions among the groups.

Global Functional Recovery After CSC Sheet Transplantation Was Enhanced by EPC Injection

Multidetector CT measured LVESV, LVEDV, and LVEF, and cardiac catheterization measured the systolic

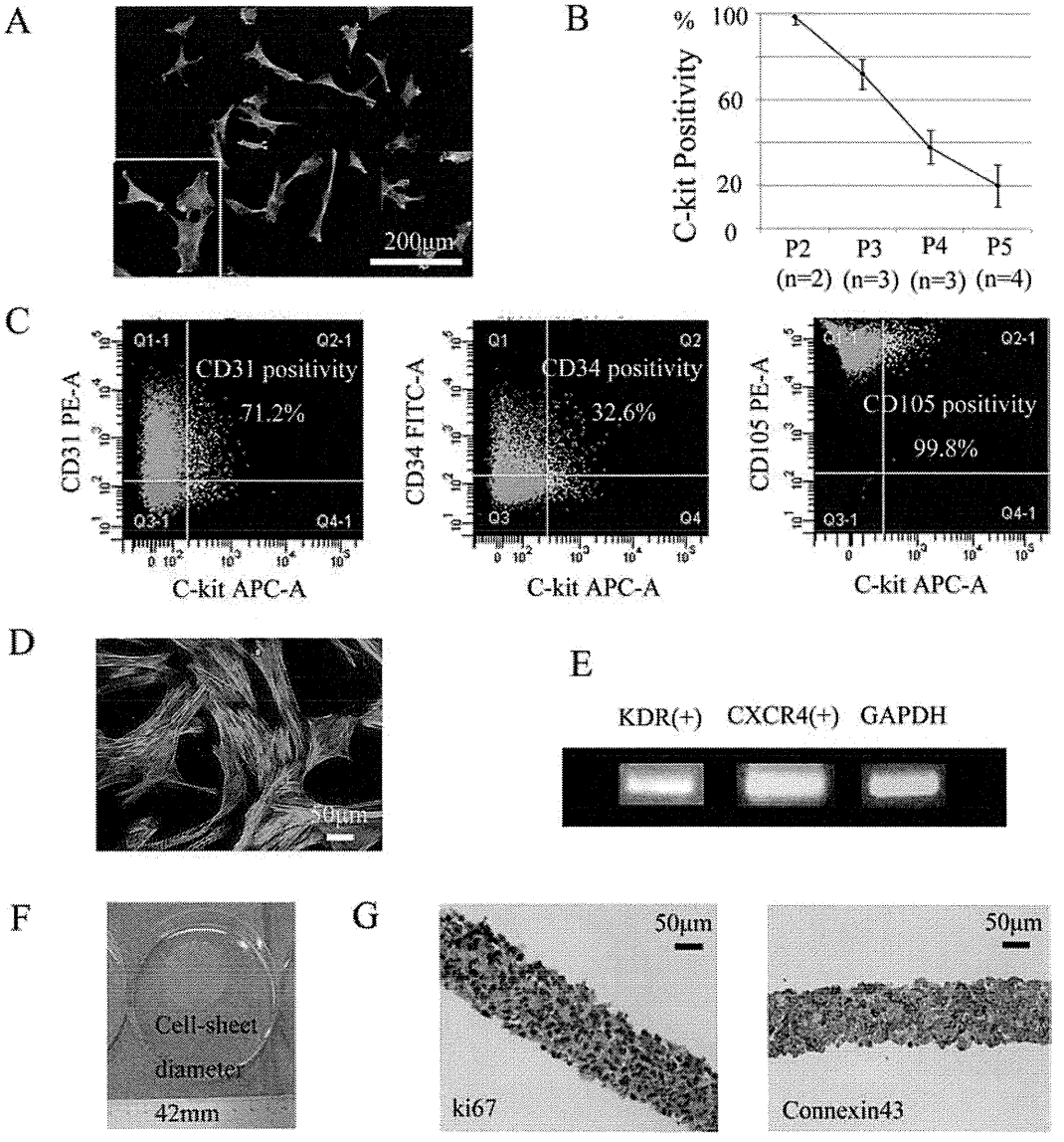

Figure 1. Characterization of the CSC sheet in vitro. (A) Representative double immunostaining for c-kit (red) and phalloidin (green) of cultured CSCs at the second passage. (B) C-Kit positivity was markedly decreased by passage culture. (C) FACS analysis of cultured CSCs at the fifth passage. (D) Cultured CSCs at the fifth passage expressed myocyte structural protein, a characteristic of cardiac progenitor cells. Phalloidin (green), troponin I (red). (E) RT-PCR analysis of CSCs at the fifth passage. (F) Detached CSC sheet. (G) Representative immunostaining for Ki-67 or connexin 43. Nuclear staining by DAPI is shown in blue in (A) and (D). Abbreviations: CSC, cardiac stem cell; FACS, fluorescence-activated cell sorting; CD31, cluster of differentiation 31; RT-PCR, reverse transcription polymerase chain reaction; KDR, kinase insert domain receptor; CXCR4, chemokine C-X-C motif receptor 4; GAPDH, glyceraldehyde 3-phosphate dehydrogenase; DAPI, 4,6-diamino-2-phenylindole.

Table 1. Evaluation of Fatal Arrhythmia by 24-h ECG Monitoring Posttransplantation

	Heart Rate (bpm)				PVC				
Group	Max Beat	Min Beat	Mean Beat	PAC	Singlet	Couplet	Triplet	VT	Vf
Sham ($n=6$)	181±42	83 (52–118)	102 (62–137)	208 (126–297)	35 (6–65)	0	0	0	0
EPC-only ($n=6$)	189±31	100 (53–132)	113 (71–163)	254 (102–377)	55 (21–83)	0	0	0	0
CSC-only ($n=6$)	171±29	55 (50–79)	97 (45–101)	120 (44–201)	19 (9–58)	0	0	0	0
CSC–EPC ($n=6$)	172±17	83 (42–92)	101 (48–169)	250 (145–377)	48 (15–77)	0	0	0	0

Abbreviations: ECG, electrocardiogram; PAC, premature atrial contraction; PVC, premature ventricular contraction; VT, ventricular tachycardia; Vf, ventricular fibrillation; EPC, endothelial progenitor cell; CSC, cardiac stem cell.

parameters d*P*/d*t* max, end-systolic pressure–volume relation (ESPVR), and diastolic parameters: τ, end-diastolic pressure (EDP), and d*P*/d*t* min. There were no significant differences in LVESV, LVEDV, or LVEF among the group pretreatment (Fig. 2A–C). The pigs treated with the sham operation developed increases in LVESV ($p<0.001$) and LVEDV ($p<0.001$) but not in LVEF (34±5% to 32±6%, $p=0.44$) in 8 weeks. In contrast, the pigs in the EPC-only or CSC-only group showed preserved LVESV (EPC-only, $p=0.23$; CSC-only, $p=0.89$), LVEDV (EPC-only, $p=0.15$; CSC-only, $p=0.13$), and LVEF (EPC-only, 37±5% to 37±4%, $p=0.91$; CSC-only, 36±4% to 43±5%, $p=0.12$). Moreover, the combined treatment induced a significant decrease in LVESV ($p=0.04$) and a significant increase in

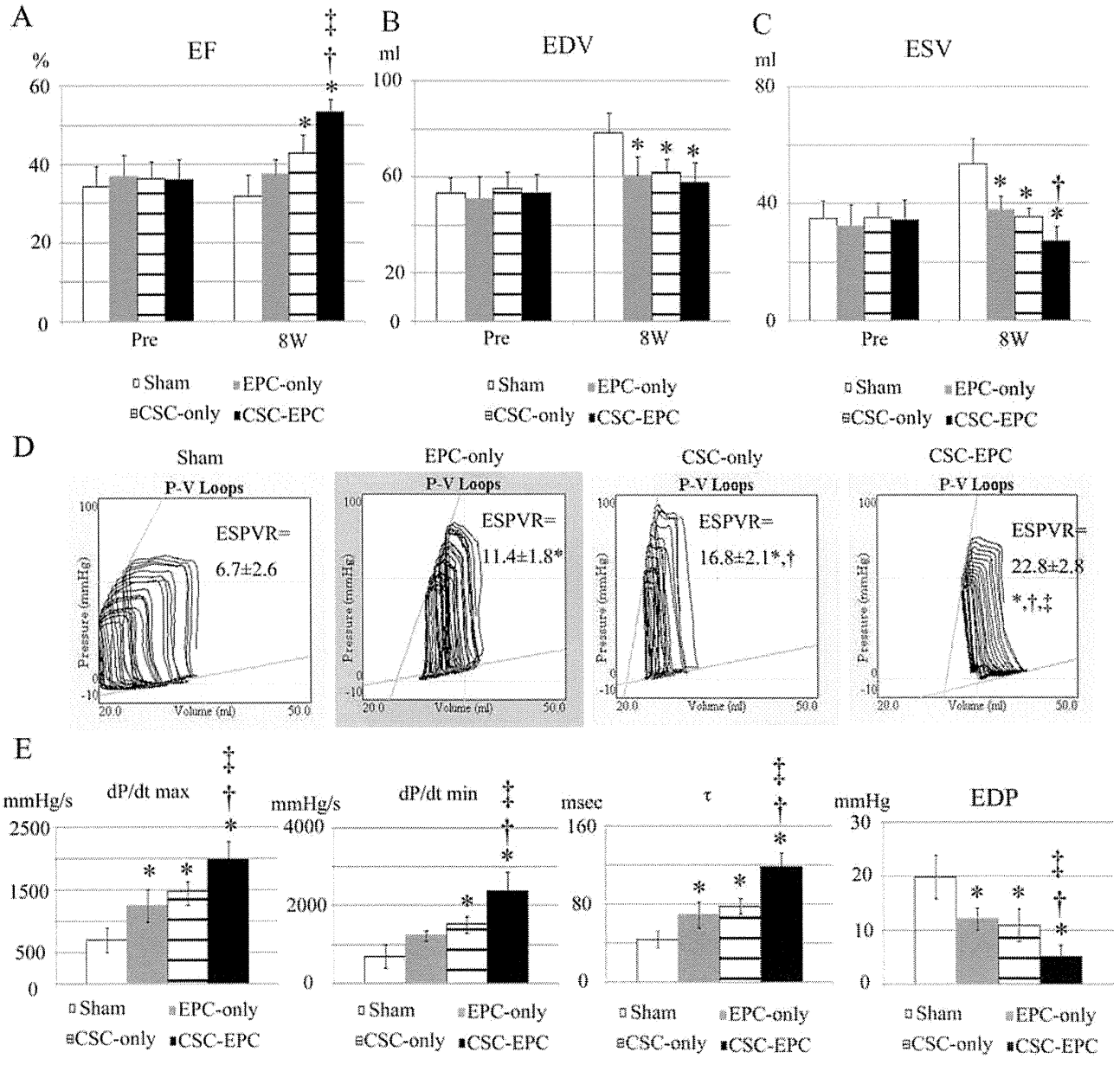

Figure 2. Global LV function assessed by multidetector CT and conductance catheter. (A–C) Multidetector CT parameters [(A) EF, (B) EDV, (C) ESV] before and 8 weeks after cell transplantation ($n=6$ each). (D) Representative P-V loops during IVC occlusion for each group at 8 weeks posttreatment ($n=5$ each). ESPVR of the CSC–EPC group was the greatest followed by that of the CSC-only group, then the EPC-only group, and then the sham group ($p<0.001$, ANOVA). (E) d*P*/d*t* max, d*P*/d*t* min, τ and EDP ($n=5$ each). *$p<0.05$ versus sham. †$p<0.05$ versus EPC-only, ‡$p<0.05$ versus CSC-only. Abbreviations: LV, left ventricle;CT, computed tomography; EF, ejection fraction; EDV, end-diastolic volume; ESV, end-systolic volume; P-V, pressure-volume; IVC, inferior vena cava; ESPVR, end-systolic pressure-volume relationship; CSC, cardiac stem cell; EPC, endothelial progenitor cell; EDP, end-diastolic pressure.

LVEF (36±5% to 53±3%, $p=0.001$) in the 8 weeks following cell transplantation.

At 8 weeks posttreatment, the LVESV of the CSC-only and EPC-only groups was significantly smaller than that of the sham group, and the LVESV of the CSC–EPC group was even smaller than that of the EPC-only group ($p<0.001$ for CSC–EPC, CSC-only, and EPC-only vs. sham, and for CSC–EPC vs. EPC-only). The LVEDV of the CSC–EPC, CSC-only, and EPC-only groups was significantly smaller than that of the sham group ($p=0.001$ for CSC–EPC, CSC-only, and EPC-only vs. sham). The LVEF of the CSC-only group was significantly greater than that of the sham group, while the LVEF of the CSC–EPC group was even greater than that of the other groups ($p<0.001$ for CSC-EPC vs. CSC-only, EPC-only, and sham, and for CSC-only vs. sham). Moreover, the ESPVR of the CSC–EPC group was the greatest, followed by that of the CSC-only group, then the EPC-only group, and then the sham group (Fig. 2D).

The dP/dt max, τ, EDP, and absolute value of dP/dt min were significantly greater in the CSC–EPC group than in the CSC-only and EPC-only groups, and these values except for the absolute value of dP/dt min were significantly greater in the CSC-only and EPC-only groups than in the sham group (Fig. 2E).

Differential Region- or Layer-Specific Effects by CSC and EPC Transplantation

Region- or layer-specific systolic LV function was assessed using speckle-tracking echocardiography, which was carried out at pretreatment and at 4 and 8 weeks posttreatment ($n=6$). There was no significant difference in the endocardial or epicardial wall motion index in the ischemic anterior area among the groups at pretreatment (Fig. 3A and B).

The pigs given the sham operation developed a significant decrease in the epicardial wall motion index (10±2% to 7±1%, $p=0.01$) and no change in the endocardial wall motion index (10±1% to 9±1%, $p=0.40$) in 8 weeks. In contrast, cell transplantation induced a significant increase in epicardial [CSC-only, 10±2% to 18 (14–28)%, $p=0.03$; CSC–EPC, 10±1% to 20±5%, $p=0.01$] and endocardial (EPC-only, 10±1% to 12±1%, $p=0.01$; CSC–EPC, 10±1% to 14±1%, $p=0.001$) indices at 8 weeks.

At 8 weeks posttreatment, the epicardial wall motion index of the CSC–EPC and CSC-only groups was significantly greater than that of the EPC-only or sham group ($p<0.001$ for CSC–EPC and CSC-only vs. EPC-only and sham) (Fig. 3A and C). In contrast, the endocardial wall motion index of the CSC–EPC group was the greatest followed by that of the EPC-only group, and both were significantly greater than that of the CSC-only or sham group ($p<0.001$ for CSC–EPC vs. EPC-only vs. CSC-only and sham) (Fig. 3B and D).

Consistent with these findings, the myocardial perfusion score in the ischemic zone at 8 weeks posttreatment was significantly greater in the CSC–EPC (36±1 dB) than in the sham group (19±2 dB, $p<0.001$) (Fig. 3E and F).

Engraftment of Transplanted CSCs and EPCs and Neovascularization of the Infarcted Wall

The engraftment of transplanted DiI-red-labeled CSCs and DiI-blue-labeled EPCs was examined, and the capillary density was assessed by fluorescence-based immunohistolabeling for vWF. At 3 weeks after cell transplantation, most of the transplanted CSCs were present over the ischemic area in the sheet shape, although no DiI-red- or DiI-blue-positive cells could be seen in any heart slice at 8 weeks posttreatment (Fig. 4A and B). The number of vWF-positive capillaries in the ischemic epicardium of the CSC–EPC and CSC-only groups was significantly greater than in the EPC-only or sham group (CSC–EPC, 251±84/mm^2; CSC-only, 257±43/mm^2; EPC-only, 105±20/mm^2; sham, 112±23/mm^2; $p=0.001$ for CSC–EPC and CSC-only vs. EPC-only and sham) (Fig. 4C). In contrast, the number of capillaries in the ischemic endocardium was significantly greatest in the CSC–EPC, followed by the EPC-only group, and then by the CSC-only or sham group (CSC–EPC, 269±11/mm^2; EPC-only, 193±14/mm^2; CSC-only, 108±30/mm^2; sham, 74±38/mm^2; $p<0.001$ for CSC–EPC vs. EPC-only vs. CSC-only and sham). In association with these findings, some of the transplanted CSCs in both the CSC–EPC and CSC-only groups were observed in native epicardial tissues, while some had migrated into the endocardial tissues only in the CSC–EPC group (Fig. 4D). On the other hand, transplanted EPCs in both the CSC–EPC and EPC groups were observed in the ischemic and peri-ischemic area of the endocardium, especially near the vascular wall.

To elucidate the possible mechanism for the transplanted CSC migration, RT-PCR and immunostaining for angiogenic growth factors were performed ($n=4$ each). The mRNA levels of swine-specific SDF-1, VEGF, and IGF-1 were upregulated in all the treatment groups (Fig. 5A). In particular, the mRNA levels of SDF-1 and the SDF-1 receptor CXCR4 were markedly greater in the CSC–EPC group than in the other groups (SDF-1 or CXCR4: $p<0.001$ for CSC–EPC vs. CSC-only, EPC-only, and sham). In addition, SDF-1, but not VEGF or IGF-1, was expressed in the cytoplasm of the transplanted CSCs that were present in the native myocardial tissue in the CSC–EPC group (Fig. 5B).

Preserved Myocardial Integrity 8 Weeks After Cell Transplantation

Interstitial fibrosis and capillary density in the heart at 8 weeks posttreatment were assessed by MT (Fig. 6A) and PAS (Fig. 6B) staining and immunohistolabeling for vWF (Fig. 6C), respectively ($n=6$ each). Excluding

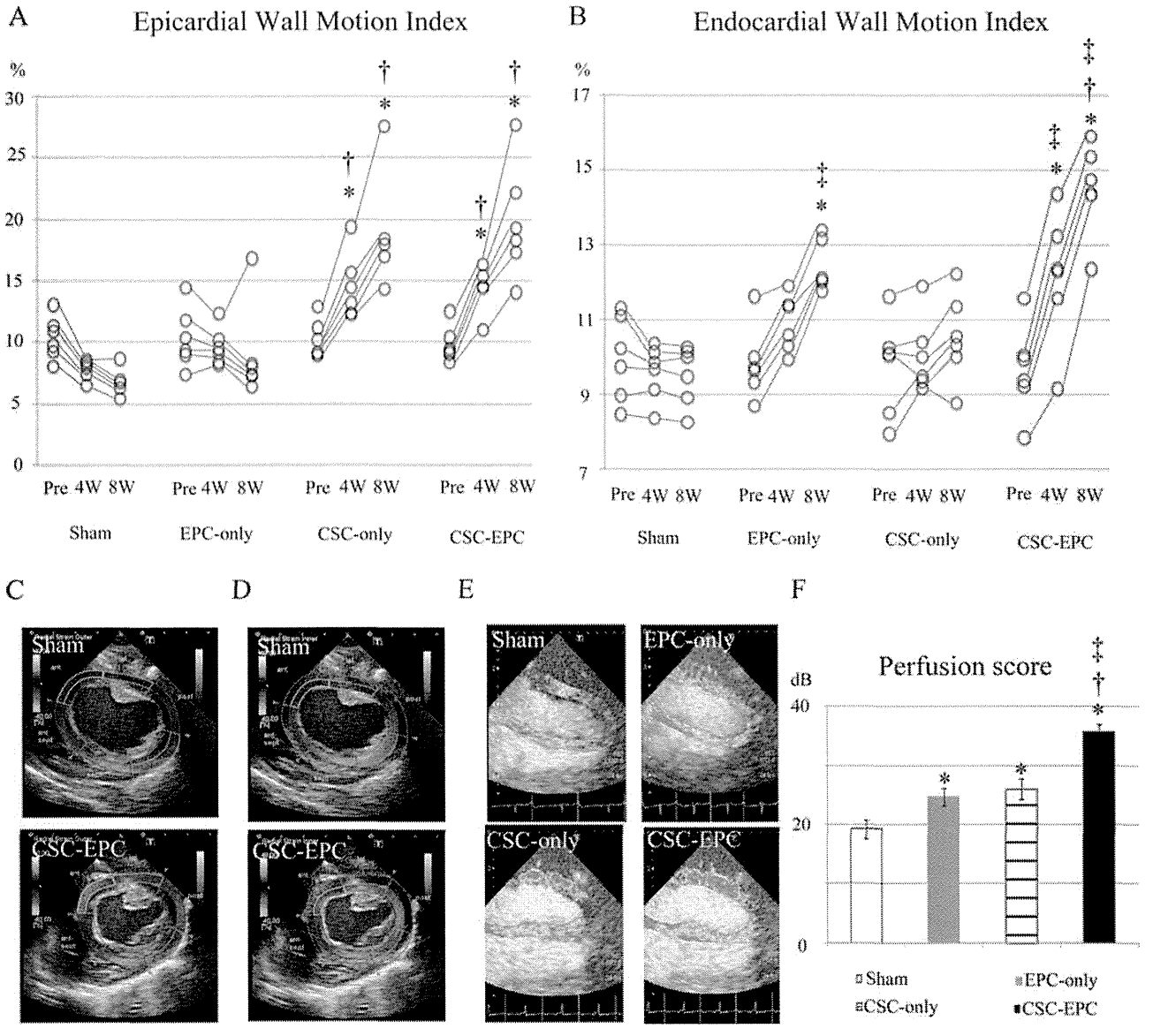

Figure 3. Region- and layer-specific systolic LV function and myocardial perfusion assessed by speckle-tracking and real-time contrast echocardiography. (A, B) Epicardial (A) and endocardial (B) WMIs in the ischemic area before, 4 and 8 weeks after cell transplantation ($n=6$ each). At 8 weeks posttreatment, the epicardial WMI of the CSC–EPC and CSC-only groups was significantly greater than that of the EPC-only or sham group ($p=0.001$, Kruskal–Wallis test), while the endocardial WMI of the CSC–EPC group was the greatest followed by that of the EPC-only group, and then the CSC-only and sham group ($p<0.001$, ANOVA). (C, D) Representative epicardial (C) and endocardial (D) radial strain images at end-systole in the CSC–EPC and sham groups. (E) Representative contrast echocardiography 2D-imaging visualized by Volmac software in each group. (F) Myocardial perfusion scores 8 weeks posttreatment ($n=6$). Myocardial perfusion score in the ischemic zone was significantly greater in the CSC–EPC than in the sham group ($p<0.001$, ANOVA) *$p<0.05$ versus sham, †$p<0.05$ versus EPC-only, ‡$p<0.05$ versus CSC-only. Abbreviations: LV, left ventricular; 2D, two-dimensional; CSC, cardiac stem cell; EPC, endothelial progenitor cell; WMI, wall motion index.

the sham group, there were no significant differences in infarct area among the other groups. On the other hand, the accumulation of collagen or area of chronic ischemic injury was the smallest in the CSC–EPC group followed by the CSC-only and EPC-only groups, and then by the sham group (CSC–EPC, 7 ± 1%; CSC-only, 15 ± 3%; EPC-only, 20 ± 3%; sham 28 ± 5%; $p<0.001$ for CSC–EPC vs. CSC-only and EPC-only vs. sham) (Fig. 6D). The LV wall thickness was significantly larger in the CSC–EPC group than in the sham group (CSC–EPC, 9 ± 1 mm; sham 7 ± 1 mm; $p<0.01$ for CSC–EPC vs. sham) (Fig. 6E).

The myocyte cell diameter at 8 weeks posttreatment was assessed in the 5-mm heart sections of the remote zone stained by PAS ($n=6$ each). The myocyte diameter

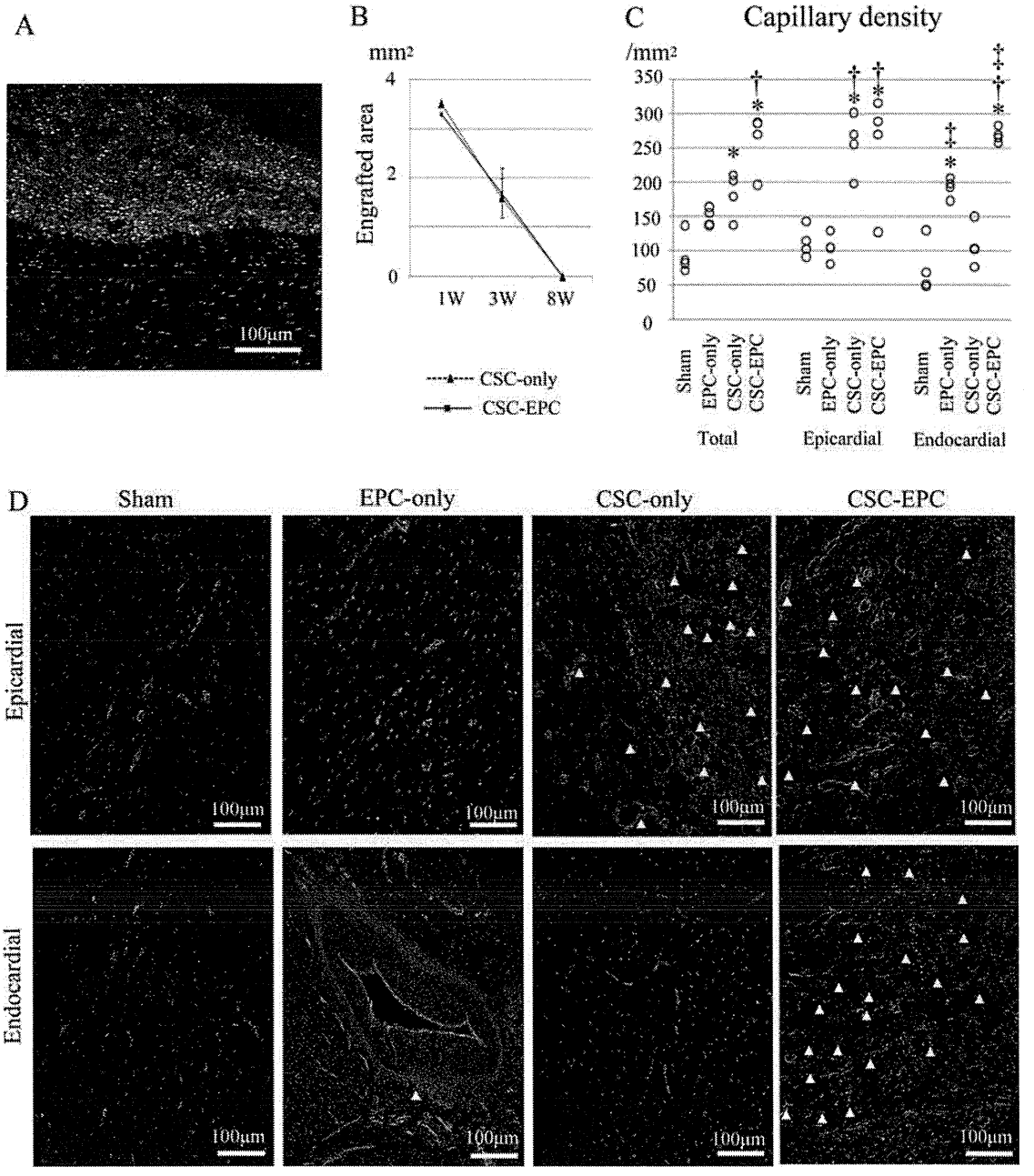

Figure 4. Engraftment of transplanted CSCs and EPCs and neovascularization of the ischemic wall. (A) Engraftment of the transplanted DiI-red-labeled CSC sheets (red) at 3 weeks posttreatment. (B) Quantification of the CSC sheet engrafted area in the CSC-only and CSC–EPC groups 1, 3, and 8 weeks posttreatment. (C) Quantification of the vWF-positive capillary density at the ischemic epicardium and endocardium in each group at 3 weeks posttreatment. The number of vWF-positive capillaries in the ischemic epicardium of the CSC–EPC and CSC-only groups was significantly greater than in the EPC-only or sham group ($p<0.001$, ANOVA), while the number of capillaries in the ischemic endocardium was significantly greatest in the CSC–EPC, followed by the EPC-only group, and then by the CSC-only and sham groups ($p<0.001$, ANOVA). (D) Representative immunostaining for vWF (green) at the ischemic epicardium and endocardium at 3 weeks posttreatment in each group. Migration of CSCs into the ischemic endocardium was observed only in the CSC–EPC group, and not in the CSC-only group. Yellow and white arrows indicate CSCs and EPCs, respectively. $^*p<0.05$ versus sham, $\dagger p<0.05$ versus EPC-only, $\ddagger p<0.05$ versus CSC-only. Nuclear staining by DAPI is shown in blue in (A) and (D). Abbreviations: CSC, cardiac stem cell; vWF, von Willebrand factor.

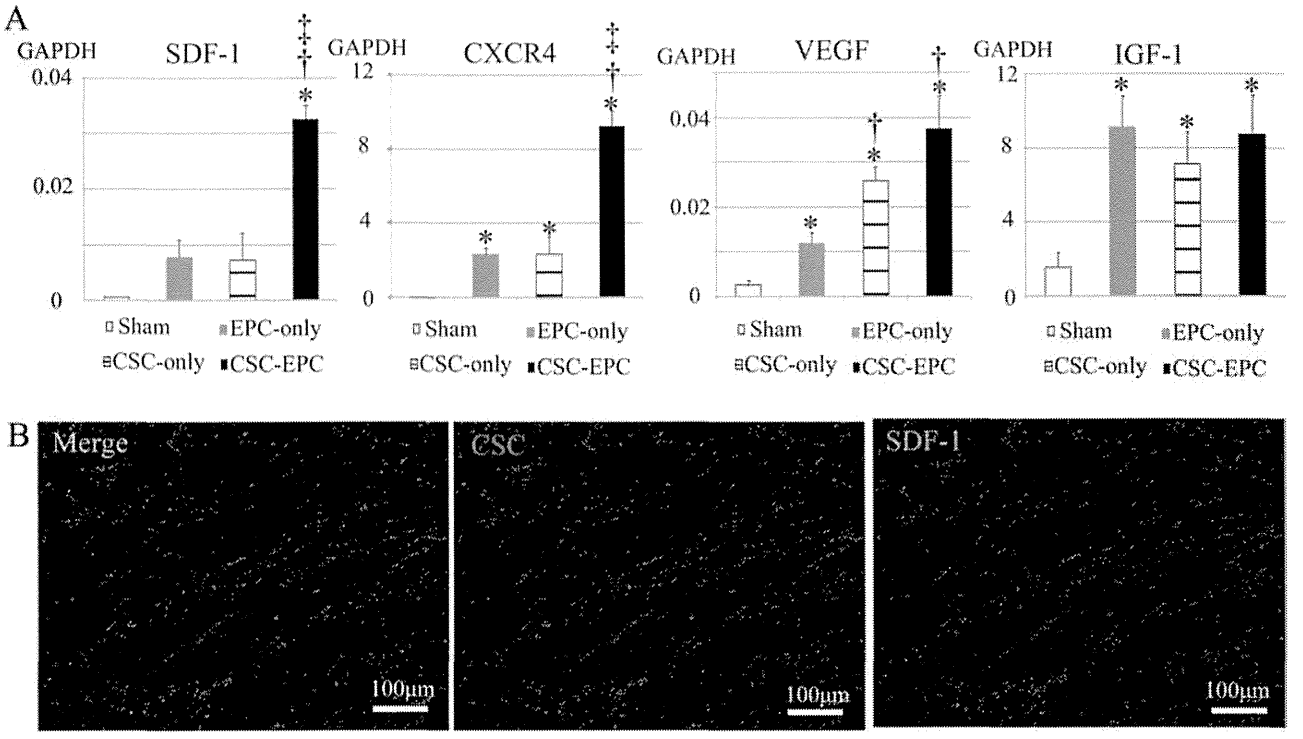

Figure 5. Possible mechanism of CSC migration. (A) RT-PCR analysis in each group at 3 weeks posttreatment. The mRNA levels of swine-specific SDF-1 ($p<0.001$, Welch's ANOVA) and CXCR4 ($p<0.001$, Welch's ANOVA) were markedly greater in the CSC–EPC group than in the other groups ($n=4$ each). (B) Representative immunostaining for SDF-1 in the CSC–EPC group at 3 weeks posttreatment. DiI-red-labeled CSCs (middle panel), SDF-1 (green) (right panel), and merged image (left panel). Nuclear staining by DAPI is shown in blue. *$p<0.05$ versus sham, †$p<0.05$ versus EPC-only, ‡$p<0.05$ versus CSC-only. Abbreviations: CSC, cardiac stem cell; RT-PCR, reverse transcription polymerase chain reaction; SDF-1, stromal cell-derived factor 1; CXCR4, chemokine C-X-C motif receptor type 4; EPC, endothelial progenitor cell; GAPDH, glyceraldehyde 3-phosphate dehydrogenase; VEGF, vascular endothelial growth factor; IGF-1, insulin-like growth factor-1.

was significantly smaller in the CSC–EPC group than in the CSC-only, the EPC-only, or the sham group (CSC–EPC, 33±9 mm; CSC-only, 49±10 mm; EPC-only, 55±8 mm; sham 61±8 mm; $p<0.001$ for CSC–EPC vs. CSC-only, EPC-only, and sham) (Fig. 6F).

The number of vWF-positive capillaries in the peri-ischemic zone of the CSC-only or EPC-only group was greater than that of the sham group, and the number of the CSC–EPC group was even greater than that of the EPC-only or sham group. (CSC–EPC, 83±11/mm^2; CSC-only, 74±6/mm^2; EPC-only, 62±8/mm^2; sham 32±10/mm^2; $p<0.001$ for CSC-only and EPC-only vs. sham, and for CSC–EPC vs. EPC-only and sham) (Fig. 6G). In addition, greater vessel formation with vascular lumen was induced in the CSC–EPC group compared with the other groups.

Phenotypic Fate of Transplanted CSCs and EPCs Posttransplantation

The phenotype of the transplanted CSCs and EPCs in the native myocardium at 8 weeks posttransplantation was histologically assessed by human- and/or swine-specific genome-based FISH analysis. Small numbers of cardiomyocytes and endothelial cells with a human genome in the nucleus were present in the native myocardium of both the CSC–EPC and CSC-only groups, but not in the EPC-only group (Fig. 7A and B). However, there was no difference in the number of cells with a human genome between the CSC–EPC and CSC-only groups. Of note, all the cells with a human genome in the nucleus also carried a swine genome in the nucleus and thus had chimeric nuclei (Fig. 7C and D).

DISCUSSION

We here demonstrated that primary c-kit-positive CSCs were successfully isolated from the human right atrium and expanded and showed that they had a differentiation potential for endothelial rather than cardiomyogenic lineages, in vitro. Human CSC sheets were successfully transplanted into the swine chronic ischemic injury heart with minimal arrhythmogenicity and elicited global functional recovery in 8 weeks. CSC sheet transplantation concomitant with intramyocardial EPC injection showed enhanced global functional recovery compared with the CSC sheet-only therapy. Transplantation of the CSC

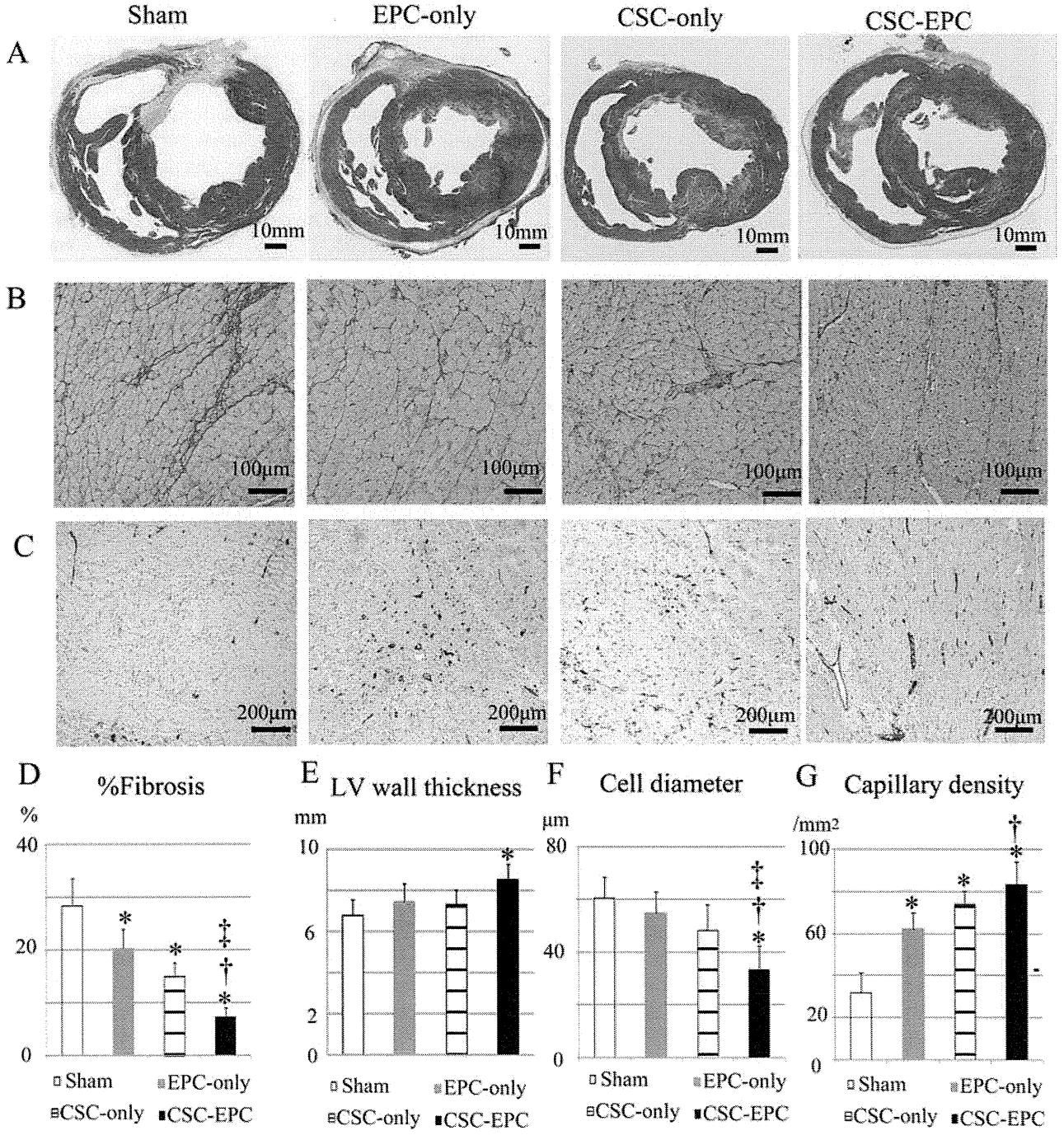

Figure 6. Histological assessment of interstitial fibrosis, capillary density, and myocyte hypertrophy 8 weeks after cell transplantation. (A) Representative Masson's trichrome staining in a section through the entire heart. (B) Representative periodic acid-Schiff staining of the remote zone. (C) Representative immunostaining for vWF in the peri-ischemic zone. (D) Quantification of fibrosis in each group ($n=6$ each). (E) In the CSC–EPC group, the thickness of the LV wall was well preserved compared with the sham group ($p<0.01$, ANOVA). (F) Quantification of the cell diameter of myocytes ($n=6$ each). (G) Quantification of capillary density at the peri-ischemic zone ($n=6$ each). The number of vWF-positive capillaries of the CSC–EPC group was the greatest, followed by the CSC-only and EPC-only groups, and then the sham group ($p<0.001$, ANOVA). *$p<0.05$ versus sham, †$p<0.05$ versus EPC-only, ‡$p<0.05$ versus CSC-only. Abbreviations: vWF, von Willebrand factor; CSC, cardiac stem cell; EPC, endothelial progenitor cell; LV, left ventricular.

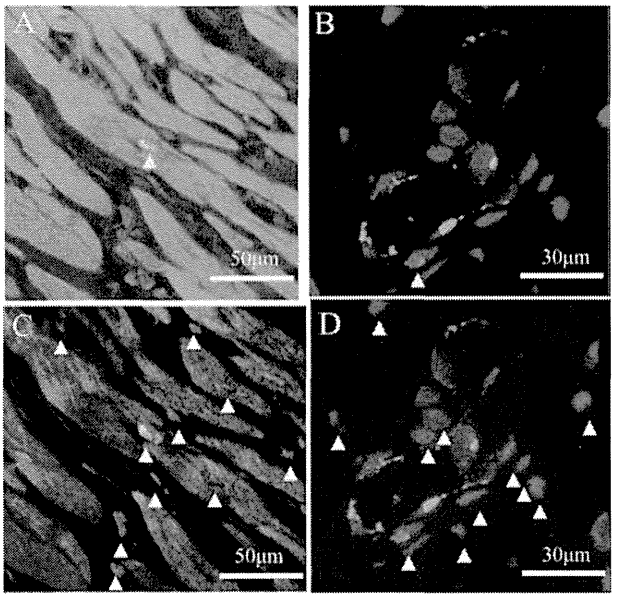

Figure 7. Phenotypic fate of transplanted CSCs and EPCs at 8 weeks posttreatment. (A, B) Representative immunostaining with human FISH (white/pink staining) and cTn-I (A; green) or vWF (B; green) in the CSC–EPC group. Small numbers of cardiomyocytes (A) and endothelial cells (B) with a human genome were present in the native myocardium. (C, D) Representative immunostaining with swine FISH and cTn-I (C) or vWF(D) in the CSC–EPC group. All the cardiomyocytes (C) and endothelial cells (D) that were positive for human genomic markers were also positive for porcine markers; thus, they had chimeric nuclei. Nuclear staining by DAPI is shown in blue. Yellow and white arrows indicate human and swine genomic markers, respectively. Abbreviations: CSC, cardiac stem cell; EPC, endothelial progenitor cell; FISH, fluorescence in situ hybridization; cTn-I, cardiac troponin I; vWF, von Willebrand factor.

sheet alone induced histological reverse LV remodeling, including attenuated interstitial fibrosis and increased vessel numbers, and concomitant EPC injection induced greater reverse LV remodeling effects than the CSC sheet-only therapy. Most of the transplanted CSCs were engrafted onto the surface over the ischemic area, while a small number migrated into the epicardium following the transplantation of the CSC sheet only. In contrast, concomitant EPC injection enhanced the migration of the transplanted CSCs into the myocardium, in association with local upregulations of SDF-1, VEGF, and IGF-1. While the CSCs of human origin in this study rarely differentiated into the cardiomyocytes in a porcine heart, transplantation of the CSCs induced functional and pathological recovery, suggesting that paracrine effects are the major therapeutic mechanisms in this study. Importantly, speckle-tracking echocardiography and histological data indicate that the CSCs and the EPCs produced different paracrine effects in the failing heart, suggesting synergic effects of these two cell types as shown in this study.

Clinical cell therapy has been reported to yield only modest functional recovery, as assessed by standard echocardiography (19,22). However, the latest echocardiographic methods, such as strain and contrast echocardiography, may better dissect layer-specific regional cardiac functions or myocardial perfusion, leading to a clearer understanding of the functional benefits of cell therapies. The adult mammalian heart is formed in three layers: contractile myocardium, inner endocardium, and outer epicardium. The layers differ in their contribution to cardiac performance and biological function (18). Myocardial infarction affects these myocardial layers to different extents, and ischemic change occurs in a wavefront pattern from the endocardium to the epicardium. In particular, the epicardium is thought to have a rich cardiac progenitor cell niche and to play an important role in cardiac repair (18,24,34). Of note, it has been shown that cell sheet implantation into the epicardium induces the expression of multiple cardioprotective factors in the heart and activates host epicardial cells crucial for cardiac repair through "crosstalk" between the implanted cell sheet and the native epicardium (20,33). This delivery method has also been demonstrated to maximize the retention and survival of the transplanted cells and to minimize the risks of cell delivery-related myocardial damage (23,27). Thus, we believed that the transplantation of CSCs by the cell sheet technique might have greater therapeutic effects in a swine chronic ischemic injury model than other delivery methods.

Our layer-specific analysis by strain echocardiography revealed that the CSC sheet transplantation induced significant functional improvement in myocardial function only in the ischemic epicardium. Consistent with this result, epicardial CSC sheet implantation induced neovascularization and reduced fibrosis in a paracrine manner in this area. We also observed the migration of transplanted CSCs into the native ischemic epicardium, which suggested that these functional and morphological benefits might be associated with the location of transplanted CSCs in the host myocardium. Previous reports demonstrated that the SDF-1–CXCR4 axis plays an important role in the migration of bone marrow and cardiac stem cells from the cell sheet to the infarct myocardium (17,28,29). Our data suggested that since migrated CSCs were located in the vicinity of SDF-1 in the host tissue, SDF-1 present in the ischemic tissue might promote the cell migration from the cell sheet to the native ischemic tissues. The strong expression of CXCR4 in the CSC sheet in vitro might support this scenario. In fact, the expressions of angiogenic growth factors, including SDF-1, in the chronic ischemic tissues were markedly diminished in the sham group, although these cytokines and adhesion molecules, which play important roles in cardiac repair after injury, are known to be abundant in

ischemic tissues at the acute stage of myocardial infarction (1). Thus, these microenvironmental factors in the host cardiac tissue might not greatly contribute to the therapeutic efficacy of the CSC sheet for the chronic ischemic injury model.

In contrast to CSC sheet transplantation, intramyocardial EPC injection significantly enhanced the improvement in myocardial function only in the ischemic and peri-ischemic endocardium, and not in the epicardium, in a paracrine manner. Urbich et al. reported that soluble factors released by EPCs promote the migration of cardiac-resident progenitor cells, using an in vitro migration assay (31). Thus, we considered that EPCs intramyocardially injected into the ischemic endocardium might promote the host tissue's expression of the angiogenic cytokine SDF-1, consequently enhancing the therapeutic efficacy of CSC sheet transplantation by improving the migration of the transplanted CSCs into the native ischemic myocardium.

The graft rate of transplanted EPCs by intramyocardial injection was lower than that of transplanted CSCs by the cell sheet technique. Transplanted CSCs were uniformly identified in the ischemic epicardium, whereas transplanted EPCs were densely located within the vascular wall of the ischemic and peri-ischemic endocardium. These different graft rates and patterns of transplanted cells might be related to the greater improvement in ESPVR and lower frequency (although not significant) of premature ventricular contraction seen in the animals receiving CSC sheet implantation alone compared with intramyocardial EPC injection alone, as previously described (20,26). One might think that EPCs could be mixed into the CSC sheet to enhance the CSCs' function; however, we have not been able to generate cell sheets from such mixed cultures. In addition, the injection of EPCs into the endocardial area might be important for attracting the migration of CSCs from the surface to the endocardial area.

In this study, contrast echocardiography dissected the improved myocardial perfusion that was seen 8 weeks after cell transplantation in all the cell therapy groups, but not the sham group. It has been shown that myocardial perfusion is impaired in chronic ischemic cardiomyopathy and that improved myocardial perfusion is associated with a suppression of LV remodeling (8). These findings indicate that the therapeutic efficacy in all the cell therapy groups might have been mainly attributable to the suppressive effects on LV remodeling. Consistent with this idea, multidetector CT showed that the increased rate of EDV between before and 8 weeks after treatment was less than 20% in all the cell therapy groups, but not in the sham group. On the other hand, invasive hemodynamic assessment using a conductance catheter also showed that CSC sheet implantation or the intramyocardial injection of EPCs significantly improved measures of LV diastolic functions, such as τ and EDP, compared with the sham operation. Previous reports demonstrated that the stiffness of the infarcted myocardium plays an important role in the postinfarction remodeling process (25). Thus, the different types of cell therapy we used may have had a softening effect on the scar tissue by increasing the cellularity, leading to a more pliable scar and less global cardiac remodeling.

In this study, in vivo CSC sheet implantation or concomitant EPC injection rarely induced the differentiation of transplanted CSCs into cardiomyogenic or vasculogenic lineages. Instead, all of the cardiac protein-expressing transplanted cells arose from fusion with existing myocytes or endothelial cells. Several lines of evidence support the idea that differentiation potential can be altered by differences in the severity of the pretreated infarct, as well as the timing of cell transplantation (20,21). In particular, Matsuura et al. reported that in viable ischemic tissues with existing cardiomyocytes, CSCs are likely to differentiate into myocytes or vascular cells via a cell fusion-dependent mechanism (20). Our layer-specific regional functional analysis by strain echocardiography identified residual viability in the ischemic area just before the cell therapies, and these conditions might have limited the differentiation potential of the CSC sheet in vivo and the ability of additional EPC injection to promote the differentiation of CSCs into the cardiomyogenic or vasculogenic lineages.

A potential limitation of this study is that the human c-kit-positive CSCs were obtained from a single donor. However, the isolation and culture methods for the primary c-kit-positive CSCs used in this study were previously established to yield CSCs of consistent functionality regardless of the donor (30). The findings of this study are therefore likely to be consistent with those obtained using CSCs from a different donor. In addition, although the swine were immunosuppressed by a previously reported regimen (15), xenogeneic cell transplantation might limit or exaggerate the therapeutic efficacy of the treatment. However, our analysis of layer-specific regional function clearly demonstrated the previously undescribed therapeutic benefit that additional EPC injection improves the CSC sheet therapy for the swine ischemic injury model.

In summary, CSC transplantation by the cell sheet technique prevented LV remodeling, through increased neovascularization and reduced fibrosis in a paracrine manner, and consequently improved the global LV function, and these effects were further enhanced by combination therapy with EPC injection. Our layer-specific strain analysis revealed that CSC sheet implantation improved regional wall motion in the epicardium, but not the endocardium. However, concomitant EPC transplantation significantly enhanced the therapeutic potential of CSC sheet

therapy in the endocardium. Concomitant EPC injection promoted migration of transplanted CSCs into the host myocardium, which might contribute to enhancement of functional recovery in the endocardium by the combination therapy. The combination of CSC sheet implantation and intramyocardial EPC injection may represent a promising strategy for ischemic cardiomyopathy.

ACKNOWLEDGMENTS: We thank Mr. Tsuyoshi Ishikawa for cell culturing and Mr. Shigeru Matsumi for excellent technical assistance for the surgery and care of the animals. This study was financially supported by a Grant-in-Aid of Scientific Research (08062134) from the Ministry of Health, Labour, and Welfare of Japan. Mr. Akima Harada is a full-time employee of CellSeed Inc., Japan. Mr. Tatsuya Shimizu and Mr. Teruo Okano are members of the scientific advisory board of CellSeed Inc., Japan. The authors declare no additional conflicts of interest.

REFERENCES

1. Abbott, J. D.; Huang, Y.; Liu, D.; Hickey, R.; Krause, D. S.; Giordano, F. J. Stromal cell-derived factor-1alpha plays a critical role in stem cell recruitment to the heart after myocardial infarction but is not sufficient to induce homing in the absence of injury. Circulation 110(21):3300–3305; 2004.
2. Adamu, U.; Schmitz, F.; Becker, M.; Kelm, M.; Hoffmann, R. Advanced speckle tracking echocardiography allowing a three-myocardial layer-specific analysis of deformation parameters. Eur. J. Echocardiogr. 10(2):303–308; 2009.
3. Becker, M.; Altiok, E.; Lente, C.; Otten, S.; Friedman, Z.; Adam, D.; Hoffmann, R.; Koos, R.; Krombach, G.; Marx, N. Layer-specific analysis of myocardial function for accurate prediction of reversible ischaemic dysfunction in intermediate viability defined by contrast-enhanced MRI. Heart 97(9):748–756; 2011.
4. Becker, M.; Ocklenburg, C.; Altiok, E.; Futing, A.; Balzer, J.; Krombach, G.; Lysyansky, M.; Kuhl, H.; Krings, R.; Kelm, M.; Hoffmann, R. Impact of infarct transmurality on layer-specific impairment of myocardial function: Amyocardial deformation imaging study. Eur.Heart J. 30(12):1467–1476; 2009.
5. Bel, A.; Planat-Bernard, V.; Saito, A.; Bonnevie, L.; Bellamy, V.; Sabbah, L.; Bellabas, L.; Brinon, B.; Vanneaux, V.; Pradeau, P.; Peyrard, S.; Larghero, J.; Pouly, J.; Binder, P.; Garcia, S.; Shimizu, T.; Sawa, Y.; Okano, T.; Bruneval, P.; Desnos, M.; Hagege, A. A.; Casteilla, L.; Puceat, M.; Menasche, P. Composite cell sheets: A further step toward safe and effective myocardial regeneration by cardiac progenitors derived from embryonic stem cells. Circulation 122(11 Suppl):S118–123; 2010.
6. Bolli, R.; Chugh, A. R.; D'Amario, D.; Loughran, J. H.; Stoddard, M. F.; Ikram, S.; Beache, G. M.; Wagner, S. G.; Leri, A.; Hosoda, T.; Sanada, F.; Elmore, J. B.; Goichberg, P.; Cappetta, D.; Solankhi, N. K.; Fahsah, I.; Rokosh D. G.; Slaughter, M. S.; Kajstula, J.; Anversa, P. Cardiac stem cells in patients with ischaemic cardiomyopathy (SCIPIO): Initial results of a randomised phase 1 trial. Lancet 378 (9806):1847–1857; 2011.
7. Dib, N.; Khawaja, H.; Varner, S.; McCarthy, M.; Campbell, A. Cell therapy for cardiovascular disease: A comparison of methods of delivery. J. Cardiovasc. Transl. Res. 4(2):177–181; 2011.
8. Galiuto, L.; Garramone, B.; Scara, A.; Rebuzzi, A. G.; Crea, F.; La Torre, G.; Funaro, S.; Madonna, M.; Fedele, F.; Agati, L. The extent of microvascular damage during myocardial contrast echocardiography is superior to other known indexes of post-infarct reperfusion in predicting left ventricular remodeling: Results of the multicenter AMICI study. J. Am. Coll. Cardiol. 51(5):552–559; 2008.
9. Hosoda, T.; Zheng, H.; Cabral-da-Silva, M.; Sanada, F.; Ide-Iwata, N.; Ogorek, B.; Ferreira-Martins, J.; Arranto, C.; D'Amario, D.; del Monte, F.; Urbanek, K.; D'Alessandro, D. A.; Michler R. E.; Anversa, P.; Rota, M.; Kajstura, J.; Leri, A. Human cardiac stem cell differentiation is regulated by a mircrine mechanism. Circulation 123(12):1287–1296; 2011.
10. Imanishi, Y.; Miyagawa, S.; Meaeda, N.; Fukushima, S.; Kitagawa-Sakakida, S.; Daimon, T.; Hirata, A.; Shimizu, T.; Okano, T.; Shimomura, I.; Sawa, Y. Induced adipocyte cell-sheet ameliorates cardiac dysfunction in a mouse myocardial infarction model: A novel drug delivery system for heart failure. Circulation 124(suppl 1):S10–S17; 2011.
11. Iwasaki, H.; Kawamoto, A.; Ishikawa, M.; Oyamada, A.; Nakamori, S.; Nishimura, H.; Sadamoto, K.; Horii, M.; Matsumoto, T.; Murasawa, S.; Shibata, T.; Suehiro, S.; Asahara, T. Dose-dependent contribution of CD34-positive cell transplantation to concurrent vasculogenesis and cardiomyogenesis for functional regenerative recovery after myocardial infarction. Circulation 113(10):1311–1325; 2006.
12. Kawaguchi, N.; Smith, A. J.; Waring, C. D.; Hasan, M. K.; Miyamoto, S.; Matsuoka, R.; Ellison, G. M. c-kit^{pos} GATA-4 high rat cardiac stem cells foster adult cardiomyocyte survival through IGF-1 paracrine signalling. PloS One 5(12):e14297; 2010.
13. Kawamoto, A.; Iwasaki, H.; Kusano, K.; Murayama, T.; Oyamada, A.; Silver, M.; Hulbert, C.; Gavin, M.; Hanley, A.; Ma, H.; Kearney, M.; Zak, V.; Asahara, T.; Losordo, D. W. CD34-positive cells exhibit increased potency and safety for therapeutic neovascularization after myocardial infarction compared with total mononuclear cells. Circulation 114(20):2163–2169; 2006.
14. Kempny, A.; Diller, G. P.; Kaleschke, G.; Orwat, S.; Funke, A.; Radke, R.; Schmidt, R.; Kerckhoff, G.; Ghezelbash, F.; Rukosujew, A.; Reinecke, H.; Scheld, H. H.; Baumgartner, H. Longitudinal left ventricular 2D strain is superior to ejection fraction in predicting myocardial recovery and symptomatic improvement after aortic valve implantation. Int. J. Cardiol. 167(5):2239–2243; 2013.
15. Kim, B. O.; Tian, H.; Prasongsukarn, K.; Wu, J.; Angoulvant, D.; Wnendt, S.; Muhs, A.; Spitkovsky, D.; Li, R. K. Cell transplantation improves ventricular function after a myocardial infarction: A preclinical study of human unrestricted somatic stem cells in a porcine model. Circulation 112(9 Suppl):I96–104; 2005.
16. Kobayashi, H.; Shimizu, T.; Yamato, M.; Tono, K.; Masuda, H.; Asahara, T.; Kasanuki, H.; Okano, T. Fibroblast sheets co-cultured with endothelial progenitor cells improve cardiac function of infarcted hearts. J. Artif. Organs 11(3):141–147; 2008.
17. Li, N.; Lu, X.; Zhao, X.; Xiang, F. L.; Xenocostas, A.; Karmazyn, M.; Feng, Q. Endothelial nitric oxide synthase promotes bone marrow stromal cell migration to the ischemic myocardium via upregulation of stromal cell-derived factor-1alpha. Stem Cells 27(4):961–970; 2009.

18. Limana, F.; Zacheo, A.; Mocini, D.; Mangoni, A.; Borsellino, G.; Diamantini, A.; De Mori, R.; Battistini, L.; Vigna, E.; Santini, M.; Loiaconi, V.; Pompilio, G.; Germani, A.; Capogrossi, M. C. Identification of myocardial and vascular precursor cells in human and mouse epicardium. Circ. Res. 101(12):1255–1265; 2007.
19. Makkar, R. R.; Smith, R. R.; Cheng, K.; Malliaras, K.; Thomson, L. E.; Berman, D.; Czer, L. S.; Marban, L.; Mendizabal, A.; Johnston, P. V.; Russell, S. D.; Schuleri, K. H.; Lardo, A. C.; Gerstenblith, G.; Marban, E. Intracoronary cardiosphere-derived cells for heart regeneration after myocardial infarction (CADUCEUS): A prospective, randomised phase 1 trial. Lancet 379(9819):895–904; 2012.
20. Matsuura, K.; Honda, A.; Nagai, T.; Fukushima, N.; Iwanaga, K.; Tokunaga, M.; Shimizu, T.; Okano, T.; Kasanuki, H.; Hagiwara, N.;Komuro, I. Transplantation of cardiac progenitor cells ameliorates cardiac dysfunction after myocardial infarction in mice. J. Clin. Invest. 119:2204–2217; 2009.
21. Matsuura, K.; Wada, H.; Nagai, T.; Iijima, Y.; Minamino, T.; Sano, M.; Akazawa, H.; Molkentin, J. D.; Kasanuki, H.; Komuro, I. Cardiomyocytes fuse with surrounding noncardiomyocytes and reenter the cell cycle. J. Cell Biol. 167(2):351–363; 2004.
22. Meyer, G. P.; Wollert, K. C.; Lotz, J.; Steffens, J.; Lippolt, P.; Fichtner, S.; Hecker, H.; Schaefer, A.; Arseniev, L.; Hertenstein, B.; Ganser, A.; Drexler, H. Intracoronary bone marrow cell transfer after myocardial infarction: Eighteen months' follow-up data from the randomized, controlled BOOST (Bone marrOw transfer to enhance ST-elevation infarct regeneration) trial. Circulation 113(10):1287–1294; 2006.
23. Miyagawa, S.; Saito, A.; Sakaguchi, T.; Yoshikawa, Y.; Yamauchi, T.; Imanishi, Y.; Kawaguchi, N.; Teramoto, N.; Matsuura, N.; Iida, H.; Shimizu, T.; Okano, T.; Sawa, Y. Impaired myocardium regeneration with skeletal cell sheets--A preclinical trial for tissue-engineered regeneration therapy. Transplantation 90(4):364–372; 2010.
24. Russell, J. L.; Goetsch, S. C.; Gaiano, N. R.; Hill, J. A.; Olson, E. N.; Schneider, J. W. A dynamic notch injury response activates epicardium and contributes to fibrosis repair. Circ. Res. 108(1):51–59; 2011.
25. Schneider, C.; Jaquet, K.; Geidel, S.; Rau, T.; Malisius, R.; Boczor, S.; Zienkiewicz, T.; Kuck, K. H.; Krause, K. Transplantation of bone marrow-derived stem cells improves myocardial diastolic function: Strain rate imaging in a model of hibernating myocardium. J. Am. Soc. Echocardiogr. 22(10):1180–1189; 2009.
26. Sekine, H.; Shimizu, T.; Dobashi, I.; Matsuura, K.; Hagiwara, N.; Takahashi, M.; Kobayashi, E.; Yamato, M.; Okano, T. Cardiac cell sheet transplantation improves damaged heart function via superior cell survival in comparison with dissociated cell injection. Tissue Eng. Part A 17(23–24):2973–2980; 2011.
27. Shimizu, T.; Sekine, H.; Yamato, M.; Okano, T. Cell sheet-based myocardial tissue engineering: New hope for damaged heart rescue. Curr. Pharm. Design 15(24):2807–2814; 2009.
28. Son, B. R.; Marquez-Curtis, L. A.; Kucia, M.; Wysoczynski, M.; Turner, A. R.; Ratajczak, J.; Ratajczak, M. Z.; Janowska-Wieczorek, A. Migration of bone marrow and cord blood mesenchymal stem cells in vitro is regulated by stromal-derived factor-1-CXCR4 and hepatocyte growth factor-c-met axes and involves matrix metalloproteinases. Stem Cells 24(5):1254–1264; 2006.
29. Tang, J. M.; Wang, J. N.; Zhang, L.; Zheng, F.; Yang, J. Y.; Kong, X.; Guo, L. Y.; Chen, L.; Huang, Y. Z.; Wan, Y.; Chen, S. Y. VEGF/SDF-1 promotes cardiac stem cell mobilization and myocardial repair in the infarcted heart. Cardiovasc. Res. 91(3):402–411; 2011.
30. Tang, X. L.; Rokosh, G.; Sanganalmath, S. K.; Yuan, F.; Sato, H.; Mu, J.; Dai, S.; Li, C.; Chen, N.; Peng, Y.; Dawn, B.; Hunt, G.; Leri, A.; Kajstura, J.; Tiwari, S.; Shirk, G.; Anversa, P.; Bolli, R. Intracoronary administration of cardiac progenitor cells alleviates left ventricular dysfunction in rats with a 30-day-old infarction. Circulation 121(2): 293–305; 2010.
31. Urbich, C.; Aicher, A.; Heeschen, C.; Dernbach, E.; Hofmann, W. K.; Zeiher, A. M.; Dimmeler, S. Soluble factors released by endothelial progenitor cells promote migration of endothelial cells and cardiac resident progenitor cells. J. Mol. Cell. Cardiol. 39(5):733–742; 2005.
32. Wollert, K. C.; Meyer, G. P.; Lotz, J.; Ringes-Lichtenberg, S.; Lippolt, P.; Breidenbach, C.; Fichtner, S.; Korte, T.; Hornig, B.; Messinger, D.; Arseniev, L.; Hertenstein, B.; Ganser, A.; Drexler, H. Intracoronary autologous bone-marrow cell transfer after myocardial infarction: The BOOST randomised controlled clinical trial. Lancet 364(9429): 141–148; 2004.
33. Zakharova, L.; Mastroeni, D.; Mutlu, N.; Molina, M.; Goldman, S.; Diethrich, E.; Gaballa, M. A. Transplantation of cardiac progenitor cell sheet onto infarcted heart promotes cardiogenesis and improves function. Cardiovasc. Res. 87(1):40–49; 2010.
34. Zhou, B.; Ma, Q.; Rajagopal, S.; Wu, S. M.; Domian, I.; Rivera-Feliciano, J.; Jiang, D.; von Gise, A.; Ikeda, S.; Chien, K. R.; Pu, W. T. Epicardial progenitors contribute to the cardiomyocyte lineage in the developing heart. Nature 454(7200):109–113; 2008.

OPEN ACCESS Freely available online

PLOS ONE

Tightly Regulated and Homogeneous Transgene Expression in Human Adipose-Derived Mesenchymal Stem Cells by Lentivirus with Tet-Off System

Hiroyuki Moriyama[1*☯], Mariko Moriyama[1,2☯], Kei Sawaragi[1], Hanayuki Okura[2], Akihiro Ichinose[3], Akifumi Matsuyama[2], Takao Hayakawa[1]

1 Pharmaceutical Research and Technology Institute, Kinki University, Higashi-Osaka, Osaka, Japan, **2** Platform for Realization of Regenerative Medicine, Foundation for Biomedical Research and Innovation, Chuo-ku, Kobe, Hyogo, Japan, **3** Department of Plastic Surgery, Kobe University Hospital, Chuo-ku, Kobe, Hyogo, Japan

Abstract

Genetic modification of human adipose tissue–derived multilineage progenitor cells (hADMPCs) is highly valuable for their exploitation in therapeutic applications. Here, we have developed a novel single tet-off lentiviral vector platform. This vector combines (1) a modified tetracycline (tet)-response element composite promoter, (2) a multi-cistronic strategy to express an improved version of the tet-controlled transactivator and the blasticidin resistance gene under the control of a ubiquitous promoter, and (3) acceptor sites for easy recombination cloning of the gene of interest. In the present study, we used the cytomegalovirus (CMV) or the elongation factor 1 α (EF-1α) promoter as the ubiquitous promoter, and EGFP was introduced as the gene of interest. hADMPCs transduced with a lentiviral vector carrying either the CMV promoter or the EF-1α promoter were effectively selected by blasticidin without affecting their stem cell properties, and EGFP expression was strictly regulated by doxycycline (Dox) treatment in these cells. However, the single tet-off lentiviral vector carrying the EF-1α promoter provided more homogenous expression of EGFP in hADMPCs. Intriguingly, differentiated cells from these Dox-responsive cell lines constitutively expressed EGFP only in the absence of Dox. This single tet-off lentiviral vector thus provides an important tool for applied research on hADMPCs.

Citation: Moriyama H, Moriyama M, Sawaragi K, Okura H, Ichinose A, et al. (2013) Tightly Regulated and Homogeneous Transgene Expression in Human Adipose-Derived Mesenchymal Stem Cells by Lentivirus with Tet-Off System. PLoS ONE 8(6): e66274. doi:10.1371/journal.pone.0066274

Editor: Niels Olsen Saraiva Câmara, Universidade de Sao Paulo, Brazil

Received December 20, 2012; **Accepted** May 2, 2013; **Published** June 12, 2013

Funding: This work was supported in part by MEXT KAKENHI Grant Number 23791304 to M.M. and 24791927 to H.M. This work was also supported in part by grants from the Ministry of Health, Labor, and Welfare of Japan and a grant from the Program for Promotion of Fundamental Studies in Health Sciences of the National Institute of Biomedical Innovation (NIBIO). The funders had no role in study design, data collection and analysis, decision to publish, or preparation of the manuscript.

Competing Interests: The authors have declared that no competing interests exist.

* E-mail: moriyama@phar.kindai.ac.jp

☯ These authors contributed equally to this work.

Introduction

Human adipose tissue–derived mesenchymal stem cells (MSCs), also referred to as human adipose tissue–derived multilineage progenitor cells (hADMPCs), are multipotent stem cells that can differentiate into various types of cells, including hepatocytes [1], cardiomyoblasts [2], pancreatic cells [3], and neuronal cells [4–6]. They can be easily and safely obtained from lipoaspirates without posing serious ethical issues and can also be expanded ex vivo under appropriate culture conditions. Moreover, MSCs, including hADMPCs, have the ability to migrate to injured areas and secrete a wide variety of cytokines and growth factors necessary for tissue regeneration [7–11]. Because of their hypoimmunogenicity and immune modulatory effects, hADMPCs are good candidates for gene delivery vehicles for therapeutic purposes [12]. Thus, hADMPCs are an attractive material for cell therapy and tissue engineering, making the development of technologies for permanent and highly controlled genetic modification of hADMPCs quite valuable.

Lentiviral vectors are powerful tools for gene transfer in primary human cells, as they integrate into the host cell genome, resulting in stable long-term transgene expression. Lentiviral vectors are less prone to transcriptional silencing than oncoretroviral vectors [13,14]; however, researchers have reported that transgene silencing occurs when a strong promoter, such as the cytomegalovirus (CMV) promoter, is used in certain cell types, especially embryonic stem cells [15–17]. Recently, it has been reported that the CMV promoter is also silenced in rat bone marrow–derived MSCs [18,19], suggesting that consideration of promoter used in the lentiviral vector is one of the most critical issues.

In addition to the choice of promoters, the specific gene expression system can have a great impact on the properties and functions of the infected hADMPCs. In order to express therapeutic genes, master regulatory genes, or microRNAs, the development of a tightly regulated, inducible gene expression system is required. The tetracycline (tet)-regulated transgene expression (tet-off) system is the most advanced system being used in gene therapy trials [20]. Two expression cassettes need to be delivered for use of the tet-off system: the regulatory unit for the constitutive expression of the transactivator (tTA), and the tet-controlled responsive unit for the expression of the gene of interest. Traditionally, these 2 cassettes should be transduced separately to establish tet-inducible cell lines. This time-consuming process

significantly limits the number of cell lines that can be generated for target gene expression. Recently, several researchers attempted to develop single-vector–based tet-inducible lentiviral systems [21–24]. However, the large plasmid size and lack of antibiotic selectable markers in these systems made the generation of plasmid constructs, high titer lentiviral particles, and stably expressing transgenic cell lines difficult.

To overcome the limitations of the current single vector-based tet-inducible lentiviral systems, we generated a robust system that incorporates all the necessary components for tet-off gene expression, restriction enzyme treatment/ligation independent cloning system, and antibiotic selectable markers in a single lentiviral vector. This vector consists of a modified tet-response element composite promoter (TRE-Tight) followed by a Gateway cassette containing *att*R recombination sites flanking a *ccd*B gene and a chloramphenicol resistant gene, which allows for easy and rapid shuttling of the gene of interest into the vector. This vector also carries an improved version of the tet-controlled transactivator (tTA-advanced) and the blasticidin resistance gene, linked by the self-cleaving viral T2A peptide, under a ubiquitous promoter. In the present study, we examined 2 ubiquitous promoters commonly used in mammalian systems: the CMV promoter and the human polypeptide chain elongation factor 1 α (EF-1α) promoter, to determine which promoter is more efficient in hADMPCs. In addition, we also confirmed whether genetically modified hADMPCs maintained their stem cell properties following transduction with this single tet-off lentiviral vector. We examined the expression pattern of cell surface markers, as well as the cells' differentiation potential into adipocytes, chondrocytes, osteocytes, and neuronal cells. Our data demonstrated that hADMPCs transduced with our all-in-one lentiviral vector were effectively selected by blasticidin without affecting their stem cell properties, and transgene expression was strictly regulated by doxycycline (Dox) not only in undifferentiated cells but also in differentiated cells. A single tet-off lentiviral vector system thus provides a powerful tool for applied research on hADMPCs.

Materials and Methods

Adipose Tissue Samples

Subcutaneous adipose tissue samples (10–50 g each) were resected during plastic surgery in 5 women (age, 20–60 years) as excess discards. The study protocol was approved by the Review Board for Human Research of Kobe University Graduate School of Medicine, Foundation for Biomedical Research and Innovation, and Kinki University Pharmaceutical Research and Technology Institute (reference number: 10-005). Each subject provided signed informed consent.

Cell Culture

hADMPCs were isolated as previously reported [1,11,25,26] and maintained in a medium containing 60% DMEM-low glucose, 40% MCDB-201 medium (Sigma Aldrich, St. Louis, MO, USA), 1× insulin-transferrin-selenium (Life technologies, Carlsbad, CA, USA), 1 nM dexamethasone (Sigma Aldrich, St. Louis, MO, USA), 100 mM ascorbic acid 2-phosphate (Wako, Osaka, Japan), 10 ng/mL epidermal growth factor (PeproTech, Rocky Hill, NJ, USA), and 5% fetal bovine serum. The cells were plated to a density of 5×10^3 cells/cm^2 on fibronectin-coated dishes, and the medium was replaced every 2 days.

Plasmid Construction and Lentivirus Production

EGFP was cloned into a pENTR11 vector (Invitrogen) to create an entry vector, pENTR11-EGFP. To generate pTRE-RfA, the tet-responsive element (TRE) of the pTRE-Tight vector (Clontech, Mountain Veiw, CA, USA) and the Reading frame A (RfA), a Gateway cassette containing *att*R recombination sites flanking a *ccd*B gene and a chloramphenicol-resistance gene (Invitrogen) were introduced into *Xba*I-*Xho*I sites of pSico (Addgene plasmid 11578). An improved version of the tet-controlled transactivator (tTA-advanced: pTet-off-advanced Clontech) was linked to the blasticidin resistance (Bsd) gene by the viral T2A peptide to generate tTA-2A-Bsd. Briefly, 2A-Bsd was amplified by PCR using the following primers:

2A-Bsd F: GGGGGATCCGGCGAGGGCAGAGGAAGTCTTCTAACATGCGGTGACGTGGAGGAAAATCCCGGGCCCATGAAGACCTTCAACATCTCTCAG, Bsd R: GCGAGATCTTTAGTTCCTGGTGTACTTG. The resultant product was confirmed by sequencing and ligation with the SmaI site of tTA. EF promoter/CMV promoter and tTA-2A-Bsd was introduced into pTRE-RfA to produce pTRE-RfA-EF-tTA-2A-Bsd or pTRE-RfA-CMV-tTA-2A-Bsd. The entry vector pENTR11-EGFP and pTRE-RfA-EF-tTA-2A-Bsd, pTRE-RfA-CMV-tTA-2A-Bsd, CSII-EF-RfA, or CSII-CMV-RfA (kindly provided by Dr. Miyoshi, RIKEN BioResource Center, Tsukuba, Japan) were incubated with LR clonase II enzyme mix (Invitrogen) to generate pTRE-EGFP-EF-tTA-2A-Bsd, pTRE-EGFP-CMV-tTA-2A-Bsd, CSII-EF-EGFP or CSII-CMV-EGFP. The resultant plasmid was mixed with packaging plasmids (pCAG-HIVg/p and pCMV-VSVG-RSV-Rev, kindly provided by Dr. Miyoshi) and transfected into 293T cells. The supernatant medium, which contained lentiviral vectors, was collected 2 days after transduction and concentrated by centrifugation (6000× *g*, 15 h, 4°C). Viral titers (transduction unit: TU) were determined by serial dilution on 293T cells and the percentage of EGFP positive cells was measured by Guava easyCyte 8HT flow cytometer (Merck-Millipore, Billerica, MA, USA).

Plasmid Propagation in *E. coli*

DH5α (F-, Φ80dlacZΔM15, Δ(lacZYA-argF)U169, deoR, recA1, endA1, hsdR17(rK-, mK+), phoA, supE44, λ-, thi-1, gyrA96, relA1) were used for general purpose. To propagate plasmids containing the ccdB gene, One Shot® ccdB Survival™ 2 T1 Phage-Resistant (T1R) chemically competent *E. coli* (Invitrogen) were used.

Western Blot Analysis

Cells were washed with ice-cold phosphate-buffered saline and lysed with M-PER Mammalian Protein Extraction Reagent (Thermo Scientific Pierce, Rockford, IL, USA). Equal amounts of proteins were separated by sodium dodecyl sulfate polyacrylamide gel electrophoresis, transferred to polyvinylidene fluoride membranes (Immobilon-P; Merck-Millipore), and probed with antibody against TetR (from Clontech). Horseradish peroxidase (HRP)-conjugated anti-mouse secondary antibody (Cell Signaling Technology, Danvers, MA, USA) was used as a probe, and immunoreactive bands were visualized with the Immobilon Western Chemiluminescent HRP substrate (Millipore). The band intensity was measured using ImageJ software.

Flow Cytometry Analysis

hADMPCs were seeded at a density of 2×10^4 cells per well in 12-well culture plates and were transduced with CSII-EF-EGFP or CSII-CMV-EGFP at a multiplicity of infection (m.o.i.) of 25, 50,

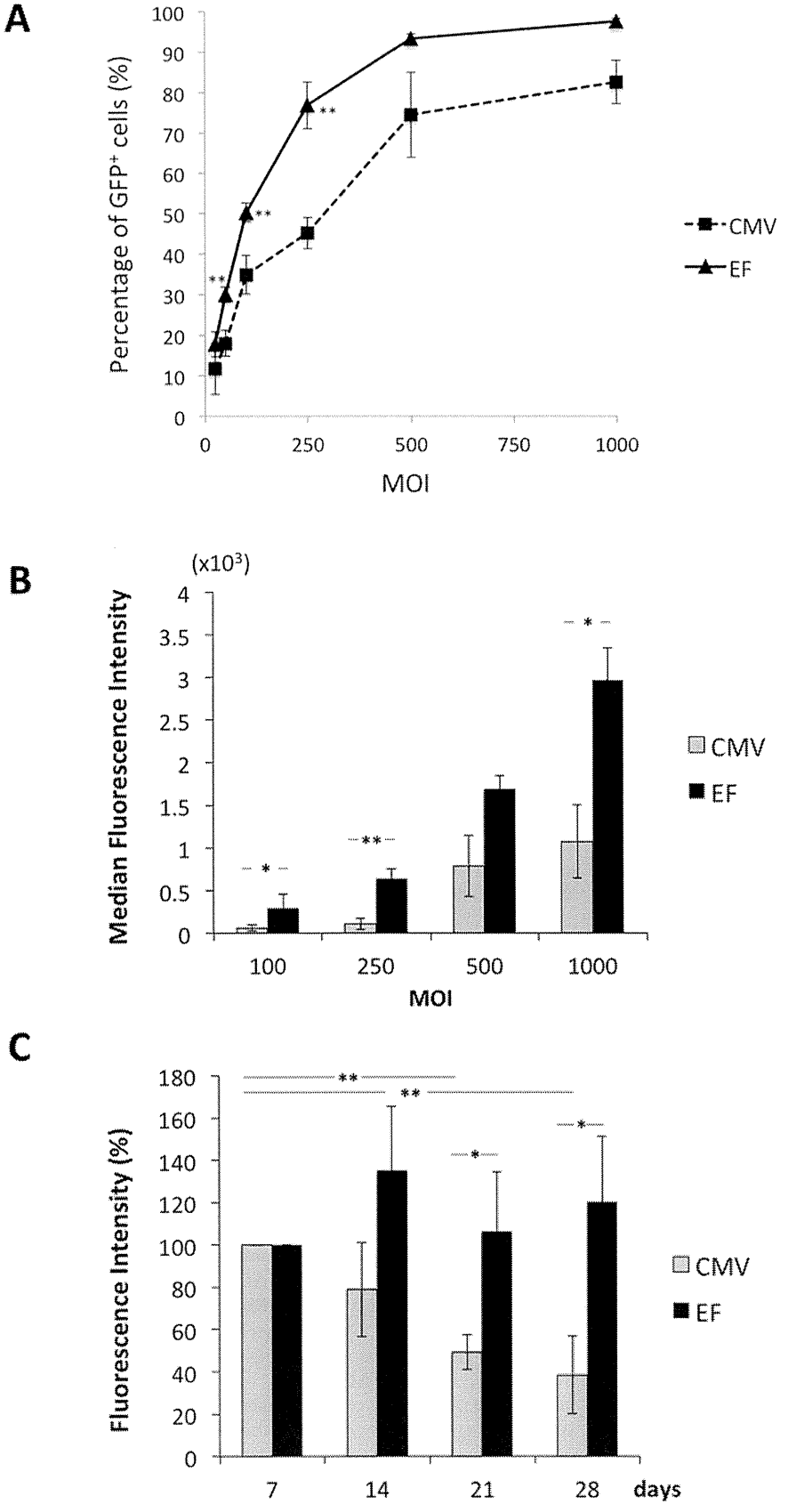

Figure 1. The efficiency of CMV or EF-1α promoter in hADMPCs. Lentiviral vectors encoding EGFP under the control of CMV or EF-1α promoter were transduced with hADMPCs at m.o.i. of 25, 50, 100, 250, 500, and 1000, and the cells were analyzed by flow cytometry. (A) The percentage of EGFP-positive hADMPCs transduced with CSII-CMV-EGFP (CMV) or CSII-EF-EGFP (EF). (B) (C) The median fluorescence intensities of the

EGFP-expressing populations. (B) hADMPCs transduced with CSII-CMV-EGFP or CSII-EF-EGFP at m.o.i. of 100, 250, 500, and 1000 were analyzed. (C) hADMPCs transduced with CSII-CMV-EGFP or CSII-EF-EGFP at m.o.i. of 1000 were analyzed over a 28 day period. Error bars represent the standard error of 3 independent analyses. **, $P<0.01$; *, $P<0.05$ (Student's t test).
doi:10.1371/journal.pone.0066274.g001

100, 250, 500, and 1000. Four days later, the cells were analyzed with a Guava easyCyte 8HT flow cytometer (Merck-Millipore) using an argon laser at 488 nm. Dead cells were excluded with the LIVE/DEAD fixable far red dead cell stain kit (Invitrogen). For analysis of hADMPCs transduced with pTRE-EGFP-EF-tTA-2A-Bsd or pTRE-EGFP-CMV-tTA-2A-Bsd, hADMPCs were transduced with the lentiviral vector at a m.o.i. of 250 and were cultured with or without 1 μg/mL Dox. Four days later, a part of the cells were analyzed with a Guava easyCyte 8HT flow cytometer. The rest of the cells were cultured with 4 μg/mL blasticidin and 1 μg/mL Dox for 3 weeks. Then, the cells were seeded in 6-well plates and cultured with or without Dox for 4 days. The cells were harvested and re-suspended in staining buffer (PBS containing 1% BSA, 2 mM EDTA, and 0.01% sodium azide) at a density of 1×10^6 cells/mL and incubated with phycoerythrin (PE)-conjugated antibody against CD13, CD29, CD34, CD44, CD73, CD90, CD105, or CD166 for 20 min. Non-specific staining was assessed using relevant isotype controls. 525/30 nm and 583/26 nm band pass filters were used for the detection of EGFP and PE, respectively. Dead cells were excluded with the LIVE/DEAD fixable far red dead cell stain kit (Invitrogen). FlowJo software (TreeStar Inc., Ashland, OR, USA) was used for quantitation analysis. The threshold for gating was determined as the fluorescence value above which less than 1% of the control cells were considered as positive events.

Fluorescence Microscopy

Phase contrast and fluorescence images were obtained using Fluorescence Microscope (BZ-9000; Keyence, Osaka, Japan) using BZ Analyzer Software (Keyence).

Adipogenic, Osteogenic, Chondrogenic, and Neurogenic Differentiation Procedures

For adipogenic differentiation, cells were cultured in differentiation medium (Zen-Bio, Durham, NC, USA). After 3 days, half of the medium was changed to adipocyte medium (Zen-Bio), and this was repeated every 3 days. Three weeks after differentiation, characterization of adipocytes was confirmed by microscopic observation of intracellular lipid droplets by oil red O staining. Osteogenic differentiation was induced by culturing the cells in DMEM containing 10 nM dexamethasone, 50 mg/dL ascorbic acid 2-phosphate, 10 mM β-glycerophosphate (Sigma), and 10% FBS. Differentiation was examined by alizarin red staining. For chondrogenic differentiation, 2×10^5 hADMPCs were centrifuged at $400\times$ *g* for 10 min. The resulting pellets were cultured in chondrogenic medium (α-MEM supplemented with 10 ng/mL transforming growth factor-β, 10 nM dexamethasone, 100 mM ascorbate, and 1× insulin–transferrin–selenium solution) for 14 days, as described previously [27]. The pellets were fixed with 4% paraformaldehyde in PBS, embedded in OCT, frozen, and sectioned at 8 μm. The sections were incubated with PBSMT (PBS containing 0.1% Triton X-100, 2% skim milk) for 1 h at room temperature, and then incubated with mouse monoclonal antibody against type II collagen (Abcam, Cambridge, MA, USA) and rabbit polyclonal antibody against GFP (Invitrogen) for 1 h. After washing with PBS, cells were incubated with Alexa 546 conjugated anti-mouse IgG and Alexa 488 conjugated anti-rabbit IgG for chondrocytes (Invitrogen) or Alexa 546 conjugated anti-rabbit IgG and Alexa 488 conjugated anti-rat IgG (Invitrogen) for neuronal cells. The cells were counterstained with 4′-6-diamidino-2-phenylindole (DAPI) (Invitrogen) to identify cellular nuclei. For neurogenic differentiation, cells were cultured in Hyclone AdvanceSTEM neural differentiation medium (Thermo Scientific, South Logan, UT, USA) for 2 days. Differentiation was examined by immunofluorescent staining against β3-tubulin. Cells were fixed with 4% paraformaldehyde in PBS for 10 min at 4°C and then washed 3 times in PBS. Blocking was performed with PBSMT for 1 h at room temperature. The differentiated cells were incubated with rabbit monoclonal antibody against β3-tubulin (Cell Signaling Technologies, Danvers, MA, USA) and rat monoclonal antibody against GFP (Nacalai, Kyoto, Japan). After washing with PBS, cells were incubated with Alexa 546 conjugated anti-rabbit IgG and Alexa 488 conjugated anti-rat IgG (Invitrogen). The cells were counterstained with 4′-6-diamidino-2-phenylindole (DAPI) (Invitrogen) to identify cellular nuclei.

Results

The Efficiency of the EF-1α Promoter was Higher than that of the CMV Promoter in hADMPCs

To determine the efficiency of the EF-1α promoter and the CMV promoter, hADMPCs were transduced with CSII-EF-EGFP or CSII-CMV-EGFP at a m.o.i. of 25, 50, 100, 250, 500, and 1000 and analyzed by flow cytometry. As shown in Figure 1A, percentage of GFP-positive cells increased in a dose-dependent manner. Intriguingly, transduction efficiency of CSII-EF-EGFP was significantly higher than that of CSII-CMV-EGFP in hADMPCs (Figure 1A). Moreover, a higher induction level of GFP was observed under the EF-1α promoter than under the CMV promoter, based on the median fluorescent intensity (Figure 1B). Furthermore, GFP fluorescent intensities driven from the CMV promoter were significantly decreased (from 100% on day 7 to 49.3% on day 21 and 38.4% on day 28; Figure 1C), indicating that promoter silencing occurred as previously reported [19]. In contrast, hADMPCs transduced with CSII-EF-EGFP sustained GFP expression levels with no significant reduction throughout the 28-day experimental period (Figure 1C).

Construction and Characterization of Dual-promoter Lentiviral Vectors in hADMPCs

Next, we constructed dual-promoter lentiviral vectors, which contain TRE-Tight followed by an improved version of tet-controlled transactivator (tTA advanced) induced under the CMV or EF-1α promoter (Figure 2A). In this "single tet-off lentiviral vector platform", the regulator and response elements are combined in a single lentiviral genome, along with a Gateway cassette containing *att*R recombination sites flanking a *ccd*B gene and a chloramphenicol-resistance gene, which allows an easy and rapid shuttling of the gene of interest into the vectors using the Gateway LR recombination reaction (Figure 2A). Using this system, we constructed pTRE-EGFP-CMV-tTA-2A-Bsd or pTRE-EGFP-EF-tTA-2A-Bsd (Figure 2B). Both the CMV and the EF-1α promoters drive the mRNA expression of tTA advanced linked to the Bsd gene by the Thosea asigna virus 2A (T2A) peptide sequence. This single transcript is then translated and cleaved into 2 proteins; tTA advanced carrying 2A tag at the

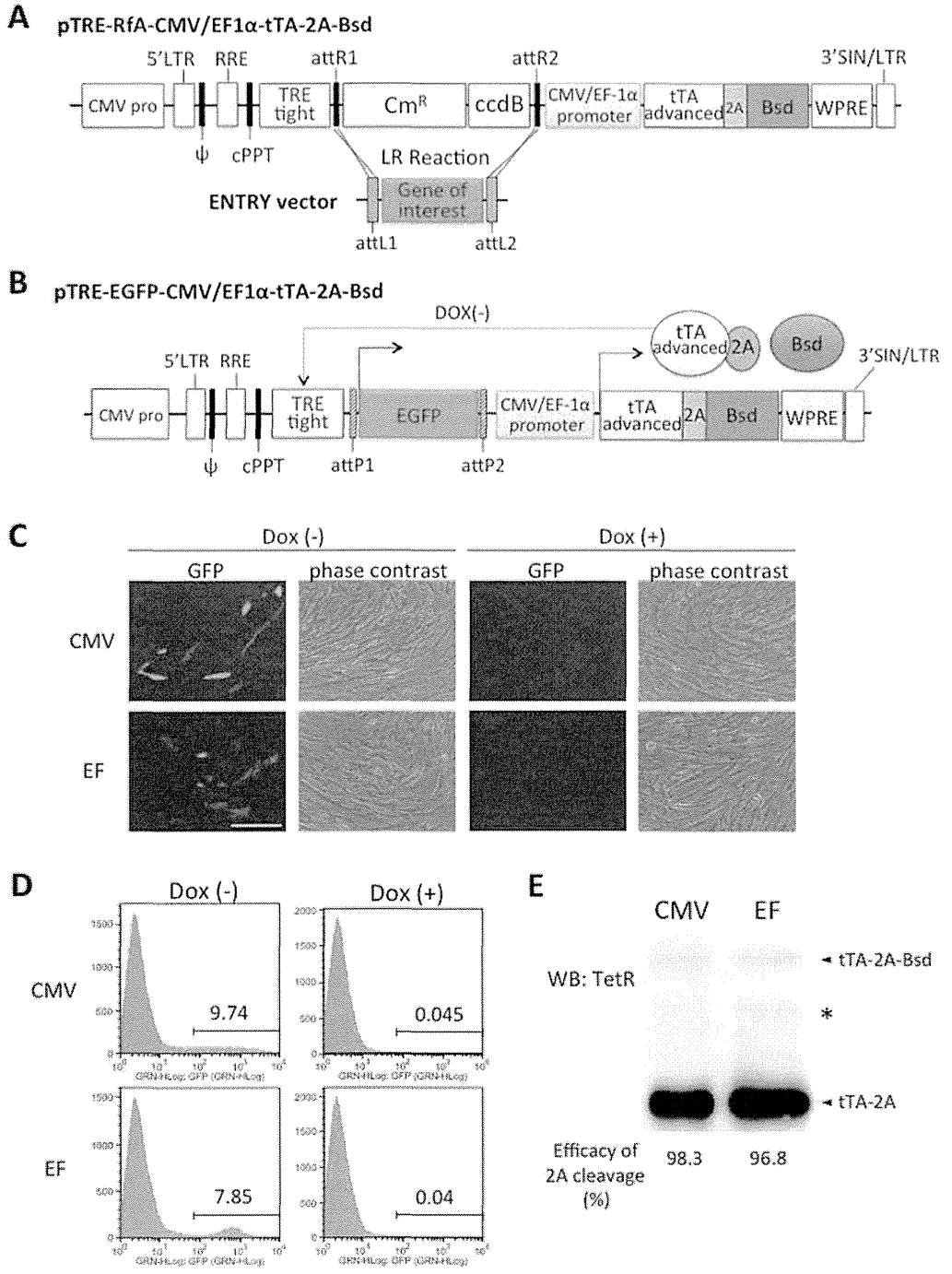

Figure 2. Schematic drawings of the single lentiviral vectors for tet-off system used in this work. (A) Gateway-compatible destination vectors containing *att*R recombination sites flanking a *ccd*B gene and a chloramphenicol-resistance gene, which allows an easy and rapid shuttling of gene of interest flanked by attL sites into the destination vectors using the Gateway LR recombination reaction. They also have an improved version of tetracycline-controlled transactivator (tTA) linked to the blasticidin resistant (Bsd) gene by the Thosea asigna virus 2A (2A) peptide sequence, whose expression is regulated by the CMV or EF-1α promoter. In the present study, we constructed an entry vector encoding EGFP flanked by attL, resulting in a destination clone, pTRE-EGFP-CMV-tTA-2A-Bsd or pTRE-EGFP-EF-tTA-2A-Bsd (B). In the absence of doxycycline (Dox), tTA-2A binds to the TRE-Tight promoter and activates EGFP transcription. For more details, see the Results section. CMV pro, CMV promoter; LTR, long terminal repeats; ψ, packaging signal; RRE, rev response elements; cPPT, central polypurine tract; TRE, tet-responsive element; Cm^R, chloramphenicol resistance; tTA, tetracycline-controlled transactivator; Bsd, blasticidin resistance; WPRE, woodchuck hepatitis virus posttranscriptional control element; SIN, self-inactivating. (C) (D) hADMPCs were transduced with pTRE-EGFP-CMV-tTA-2A-Bsd or pTRE-EGFP-EF-tTA-2A-Bsd at m.o.i. of 250. Four days after transduction, the cells were divided into 2 populations; with 1 μg/mL of Dox (Dox (+)) and without Dox (Dox (-)). (C) Fluorescent and phase contrast images. Scale bar, 200 μm. (D) Log fluorescence histograms of EGFP by flow cytometry analysis. (E) The whole cell lysates from hADMPCs transduced with pTRE-EGFP-CMV-tTA-2A-Bsd or pTRE-EGFP-EF-tTA-2A-Bsd were subjected to western blotting to monitor the cleavage efficiency of tTA-2A-Bsd proteins. A primary antibody against TetR was used to detect either tTA-2A-Bsd (non-cleaved form) or tTA-2A (cleaved form). Asterisk indicates a nonspecific band.

doi:10.1371/journal.pone.0066274.g002